Temporal and spatial variations in benthic nitrogen cycling in a temperate macro-tidal coastal ecosystem: Observation and modeling

Ratmaya Widya [1, *], Laverman Anniet M. [2], Rabouille Christophe [3], Akbarzadeh Zahra [4], Andrieux-Loyer Francoise [5], Barillé Laurent [6], Barillé Anne-Laure [7], Le Merrer Yoann [1], Souchu Philippe [1]

[1] Ifremer , LER MPL, Rue de l'Ile d'Yeu, BP 21105, 44311, Nantes, Cedex 03, France
[2] Université de Rennes, CNRS, UMR 6553 ECOBIO, Campus Beaulieu, 263 avenue du Général Leclerc, Rennes F, 35042, France
[3] Laboratoire des Sciences du Climat et de l'Environnement, CEA-CNRS UNMR 1572, Av. de la Terrasse, 91198, Gif sur Yvette, France
[4] Ecohydrology Research Group, Water Institute and Department of Earth and Environmental Sciences, University of Waterloo, 200 University Avenue West, Waterloo, Ontario, Canada
[5] Ifremer, DYNECO PELAGOS, ZI Pointe du Diable, 29280, Plouzané, France
[6] Université de Nantes, Mer Molécules Santé EA 2160, Faculté des Sciences et des Techniques, BP 92208, 44322, Nantes, Cedex 3, France
[7] Bio-Littoral, Immeuble Le Nevada, 2 Rue du Château de l'Eraudière CS 80693, 44306, Nantes, France

* Corresponding author : Widya Ratmaya, email address : widyaratmaya@gmail.com

Abstract :

We used field observations, laboratory measurements and a reactive transport model (RTM) to investigate temporal and spatial variations in benthic nitrogen (N) cycling in the eutrophic temperate macro-tidal Vilaine Bay (VB), France. A time series of benthic flux measurements and pore-water profiles of dissolved inorganic N (DIN: ammonium, nitrate, nitrite) and dissolved organic N (DON) was conducted at a single station between April and September 2015 (six times). A spatial investigation of the benthic fluxes was performed in July 2016 at this station and three other stations in the VB. All measurements were accompanied by a large panel of physical, chemical and biological descriptors in the water column. In 2015, benthic ammonium fluxes at the monitoring station varied between 75 µmol m−2 h−1 in spring and were less than 10 µmol m−2 h−1 in summer. The benthic DON fluxes co-varied with the ammonium fluxes, ranging from 100 µmol m−2 h−1 in spring to zero in summer. In the summer of 2016, a phytoplankton bloom occurred and as a result the benthic ammonium and DON fluxes reached higher values than in the spring of 2015, accompanied by bottom water hypoxia at one measured station. Benthic nitrate and nitrite fluxes varied between −31 (towards the sediments) and 22 µmol m−2 h−1 and were explained by the bottom water concentration and nitrification rates. After fitting the existing pore-water profiles, the applied RTM correctly simulated the temporal and spatial variations in the benthic DIN fluxes and predicted that a large part of the deposited organic matter (OM) is remineralized aerobically at the sediment-water interface (SWI). The overall results showed a synthetic pattern of benthic N cycling in the VB, based on the occurrence of diatom blooms as the main source of OM in the sediments. The rapid decomposition of this deposited diatom material at the SWI releases large amounts of ammonium and DON to the water

column and rapidly consumes oxygen at the sediment surface. When blooms occur in summer, their decomposition can be followed by hypoxia/anoxia in the bottom water. When blooms are absent, benthic N fluxes are weak and mainly fed by the diffusion from the pore-water. By integrating the present results in a 3D ecological model, it should be possible to more accurately predict the development of bottom water hypoxia in the VB.

Highlights

► The temporal and spatial variations of benthic N cycling in a eutrophic macro-tidal bay are studied using field measurements and the reactive transport model. ► Benthic N flux variations depend on the phytoplankton-derived organic matter input. ► Rapid mineralization of organic matter at the sediment-water interface controls benthic N cycling dynamics and sediment oxygen consumption. ► Organic matter decomposition can be followed by bottom water hypoxia when blooms occur in the summer.

Keywords : DIN, DON fluxes, diatom blooms, hypoxia/anoxia, monitoring station, reactive transport model, sediments

1. Introduction

Coastal areas are among the world's most vulnerable ecosystems to anthropogenic pressures (Turner et al., 2003), particularly to nitrogen and phosphorus pollution which leads to eutrophication (Le Moal et al., 2019). The most visible aspect of anthropogenic marine eutrophication is the mass accumulation of macroalgae on the coast (Smetacek and Zingone, 2013) and phytoplankton blooms (Carstensen et al., 2015). In shallow coastal ecosystems with water bodies exhibiting a residence time of at least several days, senescent phytoplankton blooms can be deposited at the sediment-water interface (SWI) representing a significant amount of oxidizable organic matter (OM) (Smetacek, 1980; Taguchi, 1982). When dead phytoplankton cells decompose, this sometimes results in the depletion of dissolved oxygen (O_2) in bottom waters (Cloern, 2001; Kemp et al., 2005) with a subsequent impact on the ecosystem's structure and function (Gray et al., 2002).

Nitrogen (N) is the key limiting nutrient in many coastal marine environments (Paerl, 2018). In shallow coastal ecosystems, benthic OM remineralization can represent a significant source of N in the water column, helping to maintain eutrophication (Fisher et al., 1982). During algal decomposition in sediment, OM undergoes microbially-mediated biogeochemical transformations, resulting in dissolved organic N (DON) intermediates and dissolved inorganic N (DIN) end products. These can either escape as a benthic flux across the SWI or undergo further transformation in the pore-water (Herbert, 1999; Burdige, 2001). Ammonium (NH_4^+) can be transformed into nitrite (NO_2^-) and nitrate (NO_3^-) under oxic conditions through nitrification (Ward, 2008). Under anoxic conditions, DIN (NH_4^+, NO_3^-, NO_2^-) can be eliminated as N_2 gas through denitrification and/or anammox (Thamdrup and Dalsgaard, 2002; Devol, 2015). The dissimilatory NO_3^- reduction to NH_4^+ (DNRA) competes with denitrification for NO_3^- and tends to retain N in the system (Giblin et al., 2013). The dynamics and competition between these processes govern dissolved N recycling variations and amplitudes at the SWI (Blackburn and Henriksen, 1983; Hulth et al., 2005).

Mechanisms that control benthic N cycling are complex, often site-specific and depend on several factors. These factors include: ambient nutrient concentrations in the water column (Hensen et al., 1998; Khalil et al., 2018), the amount and quality of the deposited OM (Arndt et al., 2013; Ait Ballagh et al., 2021), sediment characteristics (Blackburn and Henriksen, 1983), bottom water O_2 concentrations (Glud, 2008), temperature (Banta et al., 1995) and intensity of the sediment bioturbation (Aller and Aller, 1998), which all vary seasonally. Benthic N cycling can be highly variable over time in coastal ecosystems undergoing phytoplankton blooms (Jensen et al., 1990). In their global synthesis, Boynton et al. (2018) pointed out the lack of time series

87 measurements for a rigorous evaluation of seasonal and inter-annual variability of oxygen and

88 nutrient exchanges across the SWI in estuarine and coastal ecosystems. More generally, temporal

89 and spatial variations of benthic DIN and DON fluxes in relation with the water column

90 composition, especially chlorophyll *a* (Chl *a*) concentrations as an indicator of phytoplankton

91 biomass, still need to be investigated.

92 Numerical models are now widely used to simulate phytoplankton blooms and possible

93 hypoxia (or anoxia) under the influence of various nutrient sources and to forecast scenarios of

94 nutrient load reduction for oligotrophication purposes (Ménesguen et al., 2018). Using an

95 ecological model coupled with an early diagenetic model, Soetaert and Middelburg (2009) and

96 Gürevin et al. (2017) have shown how important it is to take benthic nutrient loads into account in

97 order to rehabilitate eutrophic coastal ecosystems. Sedimentary biogeochemical processes must be

98 considered when assessing risks of hypoxia caused by the sedimentation of phytoplankton blooms

99 (Testa et al., 2014). It is therefore essential to understand and quantify how shallow coastal

100 ecosystems accumulate, recycle and eliminate nutrients, especially at the SWI.

101 Multi-component reactive transport models (RTMs) have been widely used to estimate

102 solute exchange rates at the SWI and biogeochemical processes in both marine and freshwater

103 sediments (Wang and VanCappellen, 1996; Bohlen et al., 2011; Akbarzadeh et al., 2018), but few

104 of these models have been used to simultaneously explore temporal and spatial variations (Paraska

105 et al., 2014). The challenge remains to use a single model (e.g., same reaction parameter values)

106 that could accurately simulate benthic N fluxes and biogeochemical processes as a function of the

107 water column composition, especially phytoplankton biomass and sediment characteristics.

108 This study aims to investigate the key factors controlling the temporal and spatial variations

109 of benthic N fluxes at the SWI of a macro-tidal coastal bay threatened with eutrophication (i.e.,

110 increased phytoplankton biomass). Time-and-space-based field measurement campaigns were

111 accompanied by a large panel of physical, chemical and biological descriptors in the water column.

112 Temporal and spatial datasets were interpreted using a steady-state early diagenetic reactive

113 transport model in order to obtain a general summarized outline of the key processes governing

114 temporal and spatial variations of the benthic N fluxes in the VB.

115 **2.   Material and methods**

116 *2.1.   Study site*

117 The Vilaine Bay (VB) is a shallow macro-tidal coastal bay under direct influence of the

118 Loire and Vilaine rivers (Fig. 1, see Ratmaya et al., 2019 for a detailed description of the riverine

119 nutrient inputs). The VB has a total area of 220 km^2, with a depth varying between 10 and 15 m

120 depending on the tidal amplitude between 4 and 6 m. Water circulation is characterized by low

121 tidal and residual currents, driven mainly by tides, winds and river flows (Lazure and Jegou, 1998).

122 The water residence time in the bay varies between 10 and 20 days depending on the season and

123 can exceed 30 days during calm periods (Chapelle, 1991). The VB is one of the European Atlantic

124 coastal ecosystems most sensitive to eutrophication (Ménesguen et al., 2019), and has some of the

125 highest concentrations of chlorophyll a (Chl a) in French coastal waters (Gohin, 2011). In the VB,

126 eutrophication materializes in phytoplankton blooms, characterized by diatom dominance

127 (Ratmaya et al., 2019). The occurrence of phytoplankton blooms in this area is predominantly

128 controlled by the magnitude and timing of river floods (Guillaud et al., 2008) and is simulated

129 using a coupled pelagic biogeochemical and 3D hydrodynamic model (ECOMARS3D;

130 Ménesguen et al., 2019). Oxygen depletion in bottom waters following phytoplankton blooms is

131 frequently observed (Rossignol-Strick, 1985; Ifremer, 2015). Therefore, the onset of

132 hypoxia/anoxia in the VB is probably related to the timing of the phytoplankton blooms induced

133 by river floods. Sediments in the VB are dominated by silt (> 80%), with silty sediments mainly

134 in the north-western part of the bay, silty fine sand sediments in the eastern and north-eastern part

135 of Dumet Island, and rocky substrates (gravels) in the southern part between Dumet Island and

136 Piriac shelf (Le Bris and Glémarec, 1996).

137 *2.2. Sampling strategy*

138 *2.2.1. Water column*

139 The water quality in the VB is monitored regularly as part of the French National

140 Observation Network for Phytoplankton and Hydrology (REPHY, Belin et al., 2020) and Water

141 Framework Directive (WFD) at two monitoring stations, Nord Dumet (ND) and Ouest Loscolo

142 (OL; Fig. 1). Surface water at the ND Station has been monitored monthly (at 1 m below the

143 surface) since 2008 as part of REPHY and WFD for the nutrient and Chl a concentrations, and

144 phytoplankton composition. This station also benefits from an instrumented buoy (MOLIT),

145 deployed since 2008 to monitor the temperature, salinity, dissolved oxygen and turbidity in surface

146 and bottom waters with an hourly frequency. Surface waters at the OL station has been monitored

147 bi-monthly since 1996 for phytoplankton, nutrients and physical parameters (temperature, salinity,

148 dissolved oxygen) as part of REPHY and WFD.

149 *2.2.2. Sediment*

150 The year 2015 was devoted to a temporal study and involved renewing measurements and

151 experiments at a single station on six dates between April and September and by alternating periods

152 of strong (spring) and weak (neap) tides in order to take tidal variations into account. The ND

5

153   monitoring station (St. A, Fig. 1) was chosen for its high frequency monitoring of physicochemical

154   parameters.

155   Close to 30 stations spread over the whole bay were sampled in April 2016 to assess the

156   spatial distribution of the sediment granulometry (grain size, porosity, density), organic carbon

157   (C_{org}), total nitrogen (TN), biogenic silica (BSi) and Chl *a* contents in the first 5 cm of the

158   sediments. Spatial variations of the benthic fluxes were measured at four stations (including the

159   ND monitoring station) selected among those sampled in April 2016. All four campaigns were

160   grouped together over a short period to minimize temporal variations (July 18th to 28th).

161   *2.3.   Data acquisition*

162   *2.3.1.   River discharge*

163   River discharge data were extracted from the French hydrologic "Banque Hydro" database

164   (http://www.hydro.eaufrance.fr/, access: 20 May 2016). Daily discharge data were available at the

165   Montjean-sur-Loire gauging station for the Loire River and at the Rieux gauging station for the

166   Vilaine River.

167   *2.3.2.   Water column*

168   Physicochemical (temperature, salinity and dissolved oxygen), phytoplankton and nutrient

169   data from the ND and OL monitoring stations were used to provide a hydrological context for the

170   benthic N flux studied in 2015 and 2016. Additional samples were taken bimonthly at the ND

171   station in bottom waters (1 m above the bottom) from March to October 2015 for the nutrient and

172   Chl *a* analyses. Physicochemical data at the ND station were obtained from the MOLIT buoy, and

173   were validated and published in SEANOE (Retho et al., 2020). Water samples for the DIN and

174   DON analyses were filtered using syringe fitted filters (CA membrane 0.2 µm Sartorius$^{®}$) and

175   stored at -20°C.

176   *2.3.3.   Sediment core sampling and treatments*

177   For each sampling date, 20 undisturbed cores were collected by scuba divers using

178   Plexiglas$^{®}$ tubes (9 cm inner diameter; 30 cm height). Each core contained approximately 15 cm

179   of sediment with 1 L of overlying water. Upon collection, all sediment cores were transported to

180   the laboratory within 2 h.

181   For two sets of the triplicate sediment cores, the top first 15 cm were sliced into 10

182   horizontal layers in a glove box filled with N_2 (1 cm intervals for 0-6 cm, 2 cm intervals for 6-12

183   cm, and 3 cm intervals for 12-15 cm). The first triplicate of the sediment cores was used to extract

184   the pore-water. For each layer, the pore-water was extracted by centrifugation at 3360 *g* for 20

185   minutes at in situ temperature. The pore-water was filtered using syringe fitted filters (CA

186   membrane 0.2 µm Sartorius®) and stored at -20°C for the DIN and DON analyses. An aliquot of

187   the sediment remaining after the pore-water was collected for each layer was frozen for the C_{org}

188   and TN analyses.

189   The second triplicate of the sediment cores was used for the sediment physical property

190   analysis. For the grain size analysis, an aliquot of the wet sediment samples from each layer was

191   stored in a plastic bottle containing a mixture of one third ethanol and two thirds distilled water to

192   prevent microbial activity. Another aliquot of wet sediment of known volume and weight was

193   dried (45°C, 5d) for the density and porosity analysis. For another triplicate of the sediment cores,

194   the top first cm was sliced and frozen for the sediment Chl *a* analysis.

195   One sediment core was used to measure the vertical profiles of the dissolved O_2 at the SWI

196   and in the sediment using a miniaturized Clark-type oxygen sensor (Unisense OX500®) coupled

197   with a picoammeter (Unisense PA2000®) and a micromanipulator (Unisense MM33®) at room

198   temperature. The position of the SWI was determined visually from the O_2 microprofile according

199   to Lansard et al. (2008), by adjusting the SWI position to the steepest O_2 concentration gradient.

200   For the spatial study carried out in April 2016, the samples of the first 5 cm of the sediments

201   for the physical property analysis were lost and therefore are not presented here.

202   *2.3.4. Benthic DIN and DON fluxes*

203   For each sampling date and station, approximately 80 L of bottom water was collected

204   using a peristaltic pump for laboratory incubation experiments. When collecting bottom water

205   samples, the light intensity was also measured at 0.5 m above the bottom using a Li-COR Spherical

206   Underwater Quantum Sensor. Benthic fluxes were measured using the sediment core incubation

207   technique. For each experiment, duplicate sediment cores were incubated at in situ temperature

208   and light conditions in a thermo-regulated water bath with one duplicate wrapped with tin foil to

209   avoid light exposure. Two additional cores, containing only bottom water (blank cores), were

210   incubated in order to verify changes in the concentration in the overlying water. Each tube was

211   carefully sealed with a cap equipped with a stirring rod (Fig. S1). The overlying water was gently

212   stirred while avoiding sediment resuspension. During incubation, a probe was used to monitor O_2

213   in the overlying water in order to make sure that O_2 concentrations did not drop below 20% of the

214   initial sampling values (Dalsgaard et al., 2000). The overlying water was sampled five to six times

215   during the 20 to 24 h incubation period. Water samples were immediately filtered using syringe

216   fitted filters (CA membrane 0.2 µm Sartorius®) and stored at -20°C for analysis. The sampled

217   volume (50 mL) was replaced with the same volume from a reserve tank containing unfiltered

218   bottom water. Fluxes were calculated from the change in concentrations over the incubation time

219   after a correction for dilution due to replacing the overlying water and possible changes in the

220   blank cores. Only significant slopes (linear regression, $p < 0.05$) were taken into account, otherwise

221   the fluxes were considered to be zero. Finally, the results from light and dark measurements ($n =$

222   4) were pooled because there was no significant difference between both treatments (Mann-

223   Whitney, $p > 0.05$). At the end of incubation, sediments were fixed using 10% formalin for the

224   macrofauna counts and identification.

2.3.5. *Potential nitrification and NO_3^- reduction*

226   Potential nitrification step 1 (NH_4^+ oxidation to NO_2^-) rates were measured by incubating

227   slurries containing sodium chlorate ($NaClO_3$) in order to inhibit NO_2^- oxidation (Bianchi et al.,

228   1994; Gilbert et al., 1997). Fresh sediments (30 g) from the 0-2 cm layer were mixed

229   homogeneously with 1 L of filtered bottom water (CA membrane 0.2 µm Sartorius®) in

230   polycarbonate bottles. A control triplicate of bottles contained untreated slurries only. Two mL of

231   $NaClO_3$ (10 mM) was added to one triplicate of bottles. No substrate was added. Slurries were

232   incubated for 20 to 24 h in the dark at in situ temperature, with loosely fitted caps to ensure oxic

233   conditions. Each slurry was subsampled every 4 h, and subsamples were centrifuged (3920 g, 15

234   min). The supernatant (~10 mL) was sampled, fixed with 50 µL $HgCl_2$ (60 g L^{-1}) and stored at 4°C

235   while awaiting NO_2^- analysis. The rates were calculated using a linear regression of the change in

236   NO_2^- concentrations over time. Only significant slopes (linear regression, $p < 0.05$) were taken

237   into account, otherwise the rates were considered to be zero.

238   Potential NO_3^- reduction rates were measured using flow-through reactor methods

239   (Laverman et al., 2006). For each experiment, duplicate sediment layers (0-2 cm) were placed in

240   Plexiglas® rings (4.2 cm inner diameter; 2 cm height). A 0.2 µm pore size PVDF (Durapore®)

241   membrane filter and a glass fiber backing filter (1.2 mm thickness, 4.7 cm diameter) were placed

242   at both ends of the ring, and the resulting sediment reactor cell was enclosed by two Plexiglas®

243   caps with in/outflow channels. Reactor cells were fed with a saline solution containing NO_3^-

244   (salinity 33, 4500 µM KNO_3) using a peristaltic pump (Gilson Minipuls®) at a constant flow rate

245   (2 mL h^{-1}). The saline NO_3^- containing the input solution was bubbled with N_2 for about 10 minutes

246   to exchange and replace the existing gas phase creating an anoxic solution. Samples were collected

247   from the outflow of the reactors every 4-6 h during 20 to 24 h. Reduction rates were determined

248 from the difference in the NO_3^- concentrations at the inflow and outflow, multiplied by the flow

249 rate and normalized by the volume of the reactor.

250   The measured potential NO_3^- reduction rates (NRR) were corrected for in situ temperature

251 using the Arrhenius equation (eq. 1) and fitted to the Michaelis-Menten rate expression (eq. 2)

252 $$Pot.\,NRR_T = \frac{Pot.NRR_{Tl}}{Q_{10}^{\left(\frac{Tl-T}{10}\right)}} \tag{1}$$

253 $$R = \frac{Pot.NRR_T * [NO_3^-]}{k_{NO} + [NO_3^-]} \tag{2}$$

254 where $Pot.NRR_T$ is the potential NRR corrected with in situ temperature T, $Pot.NRR_{Tl}$ is the

255 potential NRR measured at laboratory temperature Tl, Q_{10} is a temperature coefficient ($Q10 = 2.5$;

256 Laverman et al., 2006); k_{NO} is the affinity constant of NO_3^- for denitrification (see Table S2), and

257 $[NO_3^-]$ is the average measured NO_3^- concentrations in the first 2 cm of sediment.

258 *2.3.6. Analytical methods*

259   Sediment grain size was measured using the laser diffraction technique (Malvern 2000) on

260 wet sediment samples. Density and porosity were calculated from the weight loss after drying.

261 Sediment C_{org} and TN concentrations were measured on freeze-dried sediment using a Thermo

262 Scientific™ elemental analyzer after eliminating inorganic carbon using phosphoric acid (Cauwet,

263 1975). The BSi content was determined via the alkaline extraction method using 0.1 M sodium

264 carbonate (Na_2CO_3) at 85°C (DeMaster, 1981). The extract was analyzed as dissolved silica (DSi).

265 NH_4^+, NO_3^-, NO_2^- and DSi concentrations were measured using a segmented flow colorimetric

266 analysis according to Aminot and Kérouel (2007). NO_3^- and NO_2^- concentrations in the water

267 column were reported as the sum of $NO_3^- + NO_2^-$. Total dissolved N (TDN) concentrations were

268 analyzed using the persulfate oxidation method according to Raimbault et al. (1999) after NH_4^+

269 removal (Burdige and Zheng, 1998). DON concentrations were determined from the difference

270 between TDN and DIN. Chl *a* concentrations in the water column were measured using

271 spectrophotometry according to Aminot and Kérouel (2004). Sediment Chl *a* concentrations were

272 extracted from freeze-dried sediment according to Lorenzen (1967) after an extraction with 90%

273 acetone and ultrasonication for 5 minutes (Sundbäck et al., 1996). Microscopic observations of the

274 phytoplankton and/or microalgae dominant species in the sediment surface were conducted on

275 Lugol-fixed samples collected from the uppermost mm of sediments.

276 *2.3.7. Data analysis*

9

277   If not stated otherwise, measurements are reported here as the average ± standard error:

278   triplicate cores for the potential nitrification-denitrification rates and Chl a in the sediment surface,

279   and four replicate cores for the benthic fluxes. Variations in the C_{org}, TN, DIN and DON

280   concentration profiles between sampling dates and depths were analyzed using a non-parametric

281   Kruskal-Wallis test. The inter-variable relationship was tested using a linear regression.

282   Spearman's rank correlation was used to analyze the relationship between benthic macrofauna

283   density, N transformation rates and benthic N fluxes for the temporal study carried out in 2015.

284   Bottom water turbidity and O_2 concentrations were also added to take the potential influence of

285   sediment resuspension on benthic N transformation into account. For all tests, the level of

286   significance was set to $p < 0.05$, and these tests were performed using the STATGRAPHIC

287   CENTURION software (Statgraphics Technologies Inc., Version XVIII, Released 2018). The

288   spatial distributions of C_{org}, TN, BSi and Chl a in the first 5 cm of sediment were visualized using

289   the Ocean Data View software. Automatic weighted-average gridding was used to spatially

290   interpolate the data (Schlitzer, 2002).

291   *2.4.   Reactive transport model*

292   *2.4.1. Model description*

293   A one-dimensional steady state reactive transport model (RTM) was applied to the dataset

294   mainly to simulate sediment-water DIN fluxes, as well as DIN concentrations in the pore-water

295   and to quantify N transformation process rates. This present study focuses on the sediment N cycle

296   by integrating a newly developed N reaction network as developed by Akbarzadeh et al. (2018).

297   DON benthic flux modeling was limited to only calculating the diffusive fluxes.

298   *2.4.2. Reactions*

299   This model combines general organic matter (OM) oxidation reactions with N

300   transformation processes. Five principal reactions in the sediment N cycle are considered:

301   ammonification, nitrification, denitrification, dissimilatory NO_3^- reduction to NH_4^+ (DNRA) and

302   anammox (Table S1). NH_4^+ production (ammonification) occurs by aerobic respiration,

303   denitrification, DNRA, dissimilatory iron reduction and sulfate reduction. Nitrification is modeled

304   as a two-step process: NH_4^+ (step 1) and NO_2^- (step 2) oxidation, respectively. Anaerobic processes

305   (denitrification, DNRA, anammox, $Fe(OH)_3$ and SO_4^{2-} reduction) are prevented by the presence

306   of O_2 using an inhibition term (F_{In}). Denitrification and DNRA are modeled as a one-step process

307   of OM oxidation using NO_3^-, with N_2 and NH_4^+ production, respectively, as the ultimate end result.

308   The fraction of the NO_3^- reduction by denitrification and DNRA is assumed to be a fixed value. A

309   term F_{DNRA} is added to distribute the fraction of NO_3^- reduction between two pathways (Canavan

10

310 et al., 2007; Akbarzadeh et al., 2018), and the fraction of NO_3^- reduced by denitrification is defined

311 as 1 minus (-) F_{DNRA} (Table S1). The F_{DNRA} value was adjusted by testing a series of values (5, 10,

312 25, 50, 75, 90, 95%) to obtain the fit of the NH_4^+ fluxes. The retained value was 5% (see

313 Supplement).

2.4.3. Boundary conditions and reaction parameters

315 NH_4^+, NO_3^-, NO_2^- and O_2 concentrations measured in the bottom water were set as the

316 upper boundary conditions (Table S2). This model considers two pools of organic matter: a labile

317 pool (abbreviated as OM1) and a less labile pool (abbreviated as OM2), as well as the following

318 N species: NH_4^+, NO_3^-, NO_2^-. Additional chemical species include dissolved O_2, sulfate (SO_4^{2-}),

319 dissolved iron (Fe^{2+}) and iron hydroxides ($Fe(OH)_3$). For solid species, deposition fluxes at the

320 SWI were imposed. Measured benthic fluxes for the NH_4^+ and O_2 pore-water profiles were used

321 to constrain the depositional fluxes of OM1, whereas the depositional fluxes of OM2 were adjusted

322 to best reproduce the NH_4^+ and NO_3^- pore-water profiles. A C:N ratio of 10 was assumed for OM1

323 according to the measured average C:N molar ratio sediment surface (Table S3), while that of

324 OM2 was assumed to be poorer in N (C:N = 15). The lower boundary conditions of all chemical

325 species were set to zero concentration gradients.

326 The reaction rate parameters detailed in Table S3 were obtained following a common

327 procedure in the early diagenetic modeling (e.g., Wang and VanCappellen, 1996; Canavan et al.,

328 2006; Dale et al., 2011; Akbarzadeh et al., 2018). Values were either taken directly from the

329 literature or adjusted by trial and error to obtain global fits of the model to the DIN pore-water

330 profiles and benthic flux datasets. For further details about the original model and examples of

331 applications, see Canavan et al. (2006), Couture et al. (2010), Torres et al. (2015) and Akbarzadeh

332 et al. (2018).

2.4.4. Transport

334 Solid chemical species in the simulated sediment column are transported by the sediment

335 advective velocity and particle mixing due to bioturbation, while solute chemical species are

336 additionally transported by molecular diffusion and bioirrigation. The change in concentration for

337 solute (eq. 3) and solid (eq. 4) species is described in the following mass conservation equations:

338 $$\emptyset \frac{\partial(C_d)}{\partial t} = \emptyset \frac{\partial^2(D_b C_d)}{\partial x^2} + \emptyset \frac{\partial^2(D_s C_d)}{\partial x^2} - \emptyset \omega_d \frac{\partial(C_d)}{\partial x} + \emptyset \alpha(C_{d0} - C_d) + \emptyset \sum R_d = 0 \qquad (3)$$

339 $$(1 - \emptyset)\rho \frac{\partial(C_s)}{\partial t} = (1 - \emptyset)\rho \frac{\partial^2(D_b C_s)}{\partial x^2} - (1 - \emptyset)\rho \omega_s \frac{\partial(C_s)}{\partial x} + (1 - \emptyset)\rho \sum R_s = 0 \qquad (4)$$

11

340   where C_d and C_s are the solute and solid species concentrations respectively, D_b is the bioturbation

341   coefficient ($cm^2\ yr^{-1}$), D_s is the molecular diffusion coefficient ($cm^2\ yr^{-1}$), α is the bioirrigation

342   coefficient (yr^{-1}), ρ is the sediment dry density ($g\ cm^{-3}$), ω_d and ω_s are the advective or burial

343   velocities of the pore-water and solids, respectively ($cm\ yr^{-1}$), $\emptyset$ is the sediment porosity, and R_d

344   and R_s are the reaction rates for the solute and solid species, respectively. The D_s values for all

345   solute species included in the model were corrected with the bottom water temperature and

346   sediment porosity for each measurement according to Boudreau (1997). The D_s of DON was

347   estimated using the empirical relationship between the free solution diffusion coefficient (D_o) and

348   molecular weight (MW) for various organic compounds at 25°C in distilled water reported by

349   Burdige et al. (1992), assuming a fixed average MW of 2500 Daltons. The obtained values were

350   then corrected for the in situ temperature using the Stoke-Einstein equation and transformed to D_s

351   after correction for sediment porosity (Boudreau, 1997). Bioturbation and bioirrigation were

352   described in the model by a coefficient with values that decrease with depth (Table S4).

2.4.5. Modelling strategy

354   The model was run to steady state ($\partial C/\partial t = 0$), although we are aware that coastal sediments

355   are a more transient environment than shelf or deep-sea sediments. The steady state assumption

356   was based on the calculation of diffusion time-scales of solutes calculated from the modified

357   Einstein-Smoluchowski equation (Jørgensen and Revsbech, 1985). If these time-scales are smaller

358   than the elapsed time between two campaigns, it can be assumed that the system has re-equilibrated

359   to the new condition and can be treated in a pseudo steady state. The diffusion time-scales and

360   residence time of DIN (NH_4^+, NO_3^-, NO_2^-) were estimated over the first 2 cm sediment layer, where

361   the exchange of DIN between the sediment and overlying water occurs most actively. They vary

362   from 1 to 3 days (Table S5) and from 2 to 7 days (Table S6) for the diffusion time-scales and

363   residence time, respectively, and were lower than the elapsed time between two campaigns

364   (8-15 d). The diffusion time-scales and residence time for DON were approximately six to eight

365   times greater than those for DIN (Tables S5, S6). A detailed description of the diffusion time-scale

366   calculation is provided in the Supplement.

2.4.6. Spatial simulation

368   Benthic DIN fluxes measured in July 2016 were simulated using the same fixed parameter

369   values as in 2015 (Tables S3, S4).

2.4.7. Sensitivity analyses

371   The RTM was also used as a sensitivity tool to identify the main factors (e.g., parameter

372   set, forcing functions) that exert the most effect on benthic DIN fluxes (e.g., increase, decrease or

373   direction change). The set of parameters tested were those related to environmental factors and

374   suspected to have the largest effect on SWI DIN exchanges. These include the depositional fluxes

375   of OM1, its reactivity (k_1 OM1), the proportion of OM1 and OM2, the C:N ratio of OM1,

376   bioturbation (Db), bioirrigation (α) in addition to the bottom water concentration of O_2 and NO_3^-

377   (Table S7). A stepwise approach was applied by manually changing the parameter values

378   individually and observing the model response on the NH_4^+ and NO_3^- fluxes. The model was run

379   by imposing each change in these values one by one for each sampling date of the temporal study

380   in 2015. No combination effects between the parameters were tested in the sensitivity analysis of

381   this present study. The response was calculated as a percentage of change in the NH_4^+ and NO_3^-

382   fluxes with regard to the best fits (baseline model). The contribution of NO_2^- to the DIN fluxes

383   was considered to be negligible (< 5% of the NH_4^+ and NO_3^- fluxes) and therefore they were not

384   included in the sensitivity analysis.

385   **3.   Results**

386   *3.1.   Hydrological conditions in 2015 and 2016*

387   During both studied periods (April-September 2015 and July 2016), the seasonal variations

388   of the physico-chemical parameters in the water column at both monitoring stations in the VB

389   essentially depended on climatic conditions and freshwater inputs from the Loire and Vilaine rivers

390   (Figs. 2, S2). The water column temperature varied between 10°C in March and 21°C in July with

391   temporary stratifications of several degrees in summer. The water column O_2 concentrations

392   exhibited opposite variations to those observed for temperature. The lowest bottom water O_2

393   concentration value, close to the hypoxia threshold (63 µM, Middelburg and Levin, 2009; Zhang

394   et al., 2010), was detected at St. B in July 2016 (96 µM, Table S2). Discharges from the Loire and

395   Vilaine rivers displayed similar variations in 2015 with a flood in May, while 2016 was

396   characterized by a flood from the Loire River in early June. Within one week after flooding, the

397   surface water in the VB displayed drops in salinity below 28, coinciding with the peaks of

398    $NO_3^- + NO_2^-$ concentrations (> 60 µM). Aside from these peaks, the surface and bottom water

399    $NO_3^- + NO_2^-$ concentrations were ~20 µM in spring and they gradually decreased in June to reach

400   levels below 1 µM. With regards to all four stations studied in July 2016, the highest $NO_3^- + NO_2^-$

401   concentration was recorded at St. B (Table S2). NH_4^+ concentrations remained below 2 µM in the

402   surface water. Peaks were recorded in the bottom water in May 2015 (> 5 µM) and in June 2016

403   (> 3 µM), decreasing gradually below 1 µM in July. In 2016, the highest NH_4^+ and minimum O_2

404   concentrations were found at St. B (Table S2). Chl *a* concentrations in the surface water peaked

405 ($> 15\,\mu g\,L^{-1}$) in March and May in 2015 and in June 2016 corresponding to diatom blooms. Small

406 peaks (~$5\,\mu g\,L^{-1}$) of diatom blooms were observed in August 2015 and October 2016 (see Retho,

407 2019 for additional information). For both studied periods, DON concentrations at the ND station

408 varied around $7\,\mu M$ throughout the year in both the surface and bottom waters (not shown).

409 *3.2. Sediment characteristics*

410 The sediment grain size distribution at the ND monitoring station was dominated by very

411 fine particles ($< 63\,\mu m$) and remained constant with depth regardless of the sampling date

412 (Fig. S3). At three stations sampled in July 2016, this distribution was dominated by a very fine

413 fraction ($< 63\,\mu m$) at St. B, a coarse fraction ($> 100\,\mu m$) at St. C and gravel at St. D (Fig. S4).

414 Sediment porosity and dry density varied slightly with the depth (0.85-0.79 and 2.96-2.90,

415 respectively) and sampling dates (0.80-0.82 and 2.60-2.96, respectively) at the ND station, and

416 displayed spatial variations according to the grain size distribution (Figs. S5, S6). Sediment C_{org}

417 and TN concentrations at the ND monitoring station were not significantly different according to

418 the date and depth ($p > 0.05$), with median values of 1,168 (~1.6% DW) and $120\,\mu mol\,g^{-1}$ (~0.2%

419 DW) for C_{org} and TN, respectively (Figs. 3a, 3b). The median of the C:N molar ratio varied

420 between 9.2 in the first top cm and 10.8 at depth (Fig. 3c). C_{org}, TN and BSi concentrations at the

421 sediment surface (5 cm) ranged respectively from 221 to 2,095, 25 to 233, and 10 to $215\,\mu mol\,g^{-1}$

422 and were higher in the north-western part of the bay than in the south-eastern part (Fig. S7).

423 At the ND monitoring station in 2015, the Chl *a* content in the first cm of sediment slightly

424 increased from $8.9 \pm 1.4\,\mu g\,g^{-1}$ in April to $11.9 \pm 1.5\,\mu g\,g^{-1}$ in June (Fig 2d), it decreased in August

425 ($4.6 \pm 0.3\,\mu g\,g^{-1}$) and then slightly increased in September ($8.7 \pm 0.9\,\mu g\,g^{-1}$). The highest values

426 in April and June were found subsequent to spring diatom blooms. Benthic Chl *a* displayed a

427 spatial variation similar to that of C_{org}, TN and BSi (Fig. S7), with the highest concentration

428 observed at St. B (Fig. 2h). Microscopic observations of the sediment surface in 2015 revealed

429 abundant benthic diatoms (*Pleurosigma* sp., *Navicula* spp., *Nitzschia* spp.) and organic debris in

430 April and June, while there was less organic debris, some phytoplanktonic (*Thalassiosira* sp.) and

431 tychoplanktonic (*Paralia* sp.) diatoms and many empty cells in August and September (Fig. S9).

432 Overall, on average, the macrofauna density in the incubated sediment cores of the ND monitoring

433 station in 2015 were $< 1,500\,ind.\,m^{-2}$, dominated by *Nucula nitidosa* (a small bivalve)*, Amphiura*

434 *filiformis* (a brittle star) and *Sternaspis scutata* (polychaeta) (Table S8). No significant correlations

435 were observed between the benthic macrofauna density and benthic N transformation rates, and

436 measured N fluxes (Table S9).

437 *3.3. Oxygen and dissolved N pore-water profiles*

438   Irrespective of the sampling date, the O_2 concentration decreased rapidly within the first

439   2 mm and was undetectable below this depth (Fig. 4a). In 2015, pore-water NH_4^+ concentrations

440   at the ND station showed positive concentration gradients in the first 5 cm (Fig. 4b) and nearly

441   constant values around 300 µM below 5 cm, except in two cores (June 24th and August 5th with a

442   value exceeding 1200 µM). NH_4^+ concentration profiles did not show any significant differences

443   between sampling dates ($p > 0.05$). In 2015, pore-water DON concentrations at the ND station

444   were higher than those in the bottom water, with no significant difference between sampling dates

445   ($p > 0.05$, Fig. S8a). Steep positive concentration gradients were observed in the top 1 cm, which

446   became weaker in the layer below. The global mean pore-water DON concentration was higher

447   than that of NH_4^+ in the first 5 cm layer and lower below (Fig. S8b). Pore-water NO_3^-

448   concentrations at the ND station displayed negative concentration gradients in April 2015 (Fig.

449   4c). Peaks of NO_3^- were observed in the top first 0.5 cm from June to September 2015, with a high

450   value up to 12 µM on August 5th. Pore-water NO_2^- concentrations were low (< 2 µM). Peaks of

451   NO_2^- maxima were generally observed in the first 1 cm, which decreased gradually below

452   (Fig. 4d).

453   *3.4.   Dissolved N fluxes at the SWI*

454   NH_4^+ fluxes measured at the ND station in 2015 varied between 36 ± 22 µmol m^{-2} h^{-1} in

455   April and 50 ± 19 µmol m^{-2} h^{-1} in June (Fig. 5a), and were 10 times lower in August and September

456   (5.3 ± 4.5 µmol m^{-2} h^{-1}). Maximum NH_4^+ fluxes were found after spring blooms, as observed for

457   the sediment Chl *a* content (Fig. 2d). The calculated diffusive NH_4^+ fluxes, based on pore-water

458   concentration gradients in the first cm measured in 2015, were approximately 50% of the measured

459   fluxes, with little variation over time (Table S6). In 2016, NH_4^+ fluxes were three times higher

460   than those measured in June 2015 and displayed spatial variation, with maximum values observed

461   at St. A and St. B. NH_4^+ fluxes measured at the ND station in 2015 were positively correlated to

462   the Chl *a* content in the first cm sediment layer ($r = 0.82$, $p < 0.05$, Fig. 6a). Benthic DON fluxes

463   measured at the ND station in 2015 had similar values and displayed a temporal variation similar

464   to those of NH_4^+ (Fig. 5b), with which they were positively correlated ($r = 0.82$, $p < 0.05$, Fig. 6b).

465   DON fluxes were close to zero in August and September. In 2016, the DON fluxes were in the

466   same order of magnitude as those measured in 2015. Diffusive DON fluxes represented

467   approximately 10% of the measured DON fluxes in spring and were higher in summer than in

468   spring, with little variation over the sampling dates (Table S6). At the ND station, NO_3^- fluxes

469   were directed towards the sediments in April 2015, with an average rate of -17 ± 5 µmol m^{-2} h^{-1}

470   (Fig. 5c), coinciding with high NO_3^- concentrations in the bottom water (Fig. 2c). For the rest of

471   the studied period, NO_3^- was released from the sediments except in August 2015 when the values

15

472   were close to zero (< 0.1 µmol m^{-2} h^{-1}). The release of NO$_3^-$ represented approximately 25% of the

473   NH$_4^+$ fluxes. In 2016, the measured NO$_3^-$ fluxes varied between the stations, with a flux towards

474   the sediments particularly at St. B (Fig. 5c), coinciding with high bottom water NO$_3^-$

475   concentrations (Table S2). The measured NO$_2^-$ fluxes remained below 5.0 µmol m^{-2} h^{-1}, maximum

476   values were observed in June and September in 2015 and there was a flux towards the sediments

477   at St. B in 2016 (Fig. 5d). For all benthic flux values, there was no significant difference between

478   measurements during spring and neap tides (Mann-Whitney, $p > 0.05$).

479   *3.5.   Potential nitrification and NO$_3^-$ reduction rates*

480   In 2015, the potential rates of nitrification measured at the ND station increased from April

481   to June (11.5 ± 0.4 to 28.0 ± 2.9 µmol N m^{-2} h^{-1}) and then decreased afterwards in August ($14.0 \pm$

482   2.5 µmol N m^{-2} h^{-1}) and September (12.0 ± 1.3 µmol N m^{-2} h^{-1}) to values comparable to those in

483   April (Table 2). The potential nitrification rates measured in July 2016 were lower than those

484   measured in 2015. The potential NO$_3^-$ reduction rates measured in 2015 increased from April (52.4

485   ± 6.6 µmol N m^{-2} h^{-1}) to their maximum values in June (119.0 ± 24.8 µmol N m^{-2} h^{-1}; Table 2).

486   *3.6.   Model outputs*

487   *3.6.1.   Organic matter mineralization and N transformation rates*

488   Aerobic respiration was the major pathway of labile OM (OM1) mineralization (Table 1),

489   with rates displaying similar temporal and spatial variations to those for OM1 depositional fluxes

490   (Table S2). Aerobic respiration represented up to 75% of the total rates. The anaerobic OM

491   mineralization pathway was dominated by SO$_4^{2-}$ reduction, with the highest value at St. B in 2016.

492   The reduction of NO$_3^-$ and Fe(OH)$_3$ activities was less significant (~10% of the total rates for both

493   processes). The modeled nitrification rates (step 1) were similar to the measured potential rates

494   and displayed similar temporal and spatial variations (Table 2). In 2015, the model-predicted

495   denitrification rates revealed a temporal variation contrary to the measured potential rates and

496   model-predicted nitrification rates, with the highest rates in April decreasing over the studied

497   period. In 2016, St. B displayed the highest denitrification rates. Adjusting the F_{DNRA} value to 5%

498   of all of the reduced NO$_3^-$ resulted in the best fit of the NH$_4^+$ fluxes. When values higher than 5%

499   were tested, this resulted in an overestimation of the NH$_4^+$ fluxes (Fig. S10). The anammox rates

500   were quantitatively low (< 0.2 µmol m^{-2} h^{-1}) compared to the other N transformation processes

501   with little variation over time and between stations.

502   *3.6.2.   Modeled pore-water profiles and benthic fluxes*

503   The reactive transport model reproduced a good fit for most O_2 and DIN pore-water

504   concentration profiles at the ND station in 2015 (Fig. 4). However, some discrepancies were

505   observed, such as the O_2 and NH_4^+ profiles on August 5th and September 8th, as well as the NO_3^-

506   peak on June 24th. For both studied periods (2015 and 2016), the simulated NH_4^+ and NO_3^- fluxes

507   showed a good fit with the measured fluxes (Fig. 5), with differences still observed within the

508   standard error of the measured values: 4.9, 0.6 and 9.9 $\mu M\ m^{-2}\ h^{-1}$ for NO_3^-, NO_2^- and NH_4^+ fluxes,

509   respectively.

510   *3.6.3.   Sensitivity analysis*

511   The sensitivity analysis showed that the OM1 pool input had the largest effect on the

512   magnitude of the NH_4^+ fluxes for each sampling date (Fig. 7). NH_4^+ fluxes increased with the

513   increase in OM1 input and decreased with changes in the proportion of the OM pool, which

514   corresponded to decreased OM1 fluxes by a factor of 3-4. Minor effects on the NH_4^+ fluxes were

515   observed (< 10%) for the other scenarios of change in the environmental factor-related model

516   parameters (Fig. 7). For the NO_3^- fluxes, changes in the bottom water NO_3^- concentrations and the

517   anoxic condition were the main factors influencing flux magnitude and direction (Fig. 8). In April,

518   NO_3^- sediment inward fluxes were increased by increasing the bottom water NO_3^- concentrations

519   and by eliminating O_2 from the bottom water (Figs. 8a, 8b). In June, August and September (Figs.

520   8c-8f), benthic NO_3^- fluxes reverted from outward to inward when the bottom water O_2 was set to

521   zero and the bottom water NO_3^- concentrations were increased.

522   **4.   Discussion**

523   *4.1.   OM deposition fluxes and diagenetic pathways*

524   Temporal and spatial variations of the benthic dissolved N fluxes in Vilaine Bay (VB) are

525   mainly explained by OM remineralization at the SWI. The model accurately simulated temporal

526   and spatial variations in benthic fluxes by setting high rates of OM decomposition in the upper

527   sediment layer and by essentially varying the input of labile OM (OM1), which constitutes the

528   main fraction (~80%) of the total OM depositional flux. This proportion of OM1 is comparable to

529   that obtained by a modeling study carried out on the Rhone River delta sediments (Pastor et al.,

530   2011; Ait Ballagh et al., 2021), and suggests that most OM inputs into the sediment surface in the

531   VB consists of labile matter. This fraction is characterized in the model by the first-order

532   decomposition rate constant, with this value (16 yr^{-1}) falling within the range of those values (3-

533   33 yr^{-1}) reported in Westrich and Berner (1984) from incubation experiments using fresh

534   planktonic material. The decomposition rate constant of OM2 (0.1 yr^{-1}) lies in the range of those

535   values reported in the literature (see Paraska et al., 2014; Ait Ballagh et al., 2021), which may

536   correspond to degraded algal cells, containing organic acids and lipids, with a lower degradability

537   than fresh planktonic material (Cowie et al., 1992; Komada et al., 2013). The deposition fluxes of

538   OM1 in this study (275-1,800 $\mu mol \, cm^{-2} \, yr^{-1}$) are in the range of those reported from

539   anthropogenic impacted estuarine and coastal waters, such as the Aulne and Elorn estuaries (840-

540   3,580 $\mu mol \, cm^{-2} \, yr^{-1}$; Khalil et al., 2018) , Rhône River delta (260-5,475 $\mu mol \, cm^{-2} \, yr^{-1}$; Pastor et

541   al., 2011) , and Loch Creran sea (73-1,060 $\mu mol \, cm^{-2} \, yr^{-1}$; Brigolin et al., 2009). The highest OM1

542   deposition flux values in the VB (Tables S2) correspond to the maximum Chl a contents measured

543   in the sediment surface (Fig. 2), suggesting that this OM has a plant origin (Szymczak-Żyła et al.,

544   2011).

545   The gradual decrease of O_2 and low O_2 penetration depth suggest rapid O_2 consumption

546   related to OM degradation (Pastor et al., 2011; Rabouille et al., 2021). This is consistent with our

547   model results, which indicate that OM, especially the OM1 pool, was decomposed primarily at the

548   sediment surface using O_2 (Table 1). The difference between the measured and modeled O_2

549   penetration depth on August 5th and September 8th (Fig. 4a) could not be explained by the

550   limitation of the OM input; if this is the case, the NH_4^+ fluxes would be underestimated by the

551   model. We ascribe this discrepancy to the effects of temperature on microbial metabolism related

552   to the lack of temperature control during the sediment core O_2 profiling in summer, which may

553   have increased O_2 consumption and OM mineralization (Glud et al., 1994; Mogg et al., 2017). In

554   the model, the remaining OM1 and OM2 pool was essentially mineralized through the reduction

555   of SO_4^{2-} (Table 1). This relatively high contribution of SO_4^{2-} reduction, compared to NO_3^- and

556   $Fe(OH)_3$, is in agreement with the high availability of SO_4^{2-} at the upper boundary condition

557   relative to NO_3^- and $Fe(OH)_3$ availability (Canfield, 1993). The contribution to OM decomposition

558   by SO_4^{2-} reduction increases with increasing OM deposition fluxes and particularly when the

559   bottom water O_2 concentration decreases close to the hypoxia level, as was the case at St. B in the

560   summer of 2016. This rapid oxic OM mineralization at the SWI plays a critical role in controlling

561   the bottom water O_2 concentrations as well as benthic nutrient recycling.

562   *4.2.   Benthic N transformations: dominance of aerobic processes*

563   The temporal (and spatial) variations in the benthic fluxes and pore-water concentrations

564   of NO_3^- and NO_2^- are consistent with those in the process rates and comparable to those reported

565   in coastal ecosystems subjected to seasonality with regards to the NO_3^- and NO_2^- concentrations

566   in the water column (Jensen et al., 1990; Kemp et al., 1990; Kitidis et al., 2017). The negative

567   concentration gradients of NO_3^- in April 2015, due to large NO_3^- concentrations in the water

18

568 column, are in agreement with inward sediment fluxes, which can be attributed to NO_3^- uptake via

569 denitrification (Jorgensen and Sorensen, 1988). These inward sediment NO_3^- fluxes seem

570 proportional to the NO_3^- concentrations in the bottom water. The shift in the NO_3^- flux direction

571 in June 2015 appears to be the result of increasing nitrification, as shown by the NO_3^- concentration

572 peaks in the upper 0.5 cm sediment layer and the bottom water NO_3^- depletion (Jensen et al., 1990),

573 and is in agreement with the measured potential nitrification rates. The temporal and spatial co-

574 variations between the measured potential nitrification and NO_2^- fluxes, as well as the peaks of

575 NO_2^- in the first 1 cm oxic sediment layer, emphasize the role of nitrification in benthic NO_2^-

576 production (Mordy et al., 2010).

577 Nitrification measurements using the slurry incubation of the first two cm of sediment were

578 taken without limiting O_2 and by adding substrate (NH_4^+). The good fit between the modeled

579 nitrification rates (step 1) and measurements confirms that the conditions were largely aerobic

580 during OM decomposition. The maximum nitrification rates in June suggest that nitrification is

581 dependent on the NH_4^+ produced from OM remineralization (Herbert, 1999). With regards to

582 denitrification, the model-predicted values were much lower than the potential rates measured

583 without limitation of substrate (NO_3^-), implying that denitrification was limited by the availability

584 of NO_3^- (Middelburg et al., 1996; Laverman et al., 2012). Apart from the NO_3^- supply from the

585 water column in April 2015, NO_3^- availability in the sediments was controlled by the nitrification

586 efficiency and therefore by OM remineralization, suggesting that denitrification was closely

587 coupled to nitrification (Risgaard-Petersen, 2003). This also explains the low

588 nitrification/denitrification rate values in August 2015 coinciding with the lowest OM

589 decomposition rates (Tables 1, 2). The low model-predicted DNRA rates are consistent with the

590 potential NO_3^- reduction experiments showing little NH_4^+ production, suggesting that the NO_3^-

591 reduction activity was dominated by denitrification (Laverman et al., 2012). Anammox activity is

592 generally low in eutrophic coastal waters (Bonaglia et al., 2014), which is, in our case, likely

593 related to the low availability of NO_2^- in pore-water (Dalsgaard et al., 2005). These low DNRA

594 values and annamox rates are comparable to the observations made in oxygenated surface

595 sediments from the Gulf of Finland (Jäntti et al., 2011). This dominance of aerobic processes in

596 the benthic N cycle (i.e., coupled nitrification-denitrification), as for aerobic OM mineralization,

597 suggests that the transformation of N in the VB occurs mainly in the uppermost centimeter of the

598 sediments.

599 *4.3.   Importance of DON in benthic N cycling*

19

600   The DON pore-water concentrations in the VB sediments are within the same range as the

601   DIN (mainly NH_4^+) concentrations and are in the same order of magnitude as those reported in the

602   Chesapeake Bay (Burdige and Zheng, 1998) and the St. Lawrence estuary (Alkhatib et al., 2013).

603   The concentration gradients in the DON pore-water profiles were lower than those of NH_4^+ below

604   a depth of 2 cm (Fig. S7), suggesting that DON below this sediment layer may largely consist of

605   refractory compounds slowly producing NH_4^+ in the pore-water (Burdige, 2001; Burdige et al.,

606   2016). The absence of a temporal variation in the DON pore-water profiles indicates that DON

607   cycling in the pore-water, as for NH_4^+ (see below), is relatively independent of seasonal events in

608   the water column, particularly fresh OM inputs from phytoplankton blooms (Hansen and

609   Blackburn, 1992). The positive concentration gradients in the upper 1 cm layer imply DON

610   production and release to the overlying water by diffusion (Alkhatib et al., 2013). However, the

611   weak concentration gradient in the DON pore-water profiles below a depth of 2 cm and much

612   higher DON diffusion time-scales and residence time than those of DIN converge to explain low

613   diffusive DON fluxes (see the Supplementary Material). As observed for NH_4^+ (see below),

614   temporal variations in the diffusive DON fluxes did not reflect large fluctuations in the measured

615   fluxes via incubation.

616   The benthic DON fluxes measured in the VB represent up to 50% of the dissolved N fluxes

617   (Fig. 5). Although data on benthic DON flux measurements remain scarce in the literature, it

618   appears that their values become truly quantifiable only after the sedimentation of fresh OM

619   (Burdige and Komada, 2002; Eyre and Ferguson, 2002). Parallel temporal and spatial variations

620   in the benthic DON and NH_4^+ fluxes infer that DON was released during OM degradation in the

621   sediment surface. Our measurements confirm those of Hansen and Blackburn (1992), showing that

622   the addition of diatom material to the sediment during laboratory experiments leads to a release of

623   DON to the overlying water, as significant as that of NH_4^+. However, the importance of DON

624   fluxes in benthic N cycling dynamics remains understudied in early diagenetic modeling studies

625   (Paraska et al., 2014). This omission of DON in the RTM is likely related to the uncertainty in

626   estimating its diffusion coefficient (Alperin et al., 1999; Alkhatib et al., 2013), as well as to the

627   scarcity of data concerning benthic DON fluxes and pore-water concentrations (Boynton et al.,

628   2018). Given the significance of DON release in this study, the integration of DON in the RTM

629   may constitute an improvement in order to better estimate the role of this compound in the benthic

630   N budget.

631   *4.4.   Phytoplankton-derived OM mineralization at the SWI as the main driver of benthic N fluxes*

632   The benthic NH_4^+ fluxes measured in the VB showed strong temporal and spatial

633   variations, with values lying within the range of those reported in other coastal ecosystems

634   (Boynton et al., 2018). The exchange of NH_4^+ at the SWI can be influenced by several processes,

635   in particular: consumption by benthic primary producers, benthic macrofauna activities, diffusive

636   exchanges between the pore-water and overlying water and direct release from the decomposition

637   of OM that was deposited at the SWI. These processes largely depend on hydrodynamic conditions

638   (water aeration, sediment resuspension, etc.) and OM inputs (production at the SWI and

639   sedimentation).

640   Primary producers that develop at the SWI (e.g., macroalgae and microphytobenthos) can

641   assimilate NH_4^+ produced in the sediment and affect its exchange between the sediment and

642   overlying water (Sundbäck et al., 2006). In the VB, the presence of macroalgae is limited to the

643   rocky bottom and to the edge and foreshore, both representing less than 10% of the total surface

644   area of the bay (Ehrhold, 2014). Microphytobenthos and particularly benthic diatoms can develop

645   when sufficient light reaches the sediment surface (Miller et al., 1996). The absence of a significant

646   difference between benthic flux measurement values under light and dark conditions in our

647   experiment suggests that microphytobenthos had a minor contribution to the benthic fluxes. The

648   high water column turbidity in the VB (Tessier et al., 2011), which limits microphytobenthos

649   development (Mangan et al., 2020), may explain this hypothesis.

650   Benthic macrofauna rework sediments, favoring their homogenization and oxygenation,

651   and accelerating the remineralization of sedimentary OM (Shull, 2019). The excretion of dissolved

652   N by benthic macrofauna can also contribute to the enrichment of pore- water and overlying waters

653   with NH_4^+ and DON (Gardner et al., 1993; Yamamuro and Koike, 1998). Among the three main

654   taxa observed in the incubated cores, *Amphiura filiformi*s and *Sternaspis scutata* may favor

655   biodiffusion, whereas *Nucula nitidosa* is instead considered to be a surficial modifier (Queiros et

656   al., 2013). Although the densities of these three species are moderate in the VB (Le Bris and

657   Glémarec, 1996; Ehrhold et al., 2008), they probably enhanced sedimentary OM recycling (Follum

658   and Gray, 1987). The exceptionally high NH_4^+ concentrations in two cores (June 24th and

659   August 5th), found also for phosphate and silicate (Ratmaya, 2018), could be explained by

660   heterogeneities linked to macrofaunal activity. However, no significant correlations between

661   macrofauna density and benthic N transformation rates or N fluxes were found. Additionally, the

662   low bioturbation and bioirrigation coefficients used in the model were sufficient to adjust benthic

663   DIN fluxes, which may indicate the minor influence of benthic macrofaunal activities on benthic

664   N cycling. Although the contribution of benthic macrofauna to benthic dissolved N fluxes could

665   not be quantified in this study, it probably represents a limited part of the fluxes from the sediment
666   to the water column, but this still needs to be confirmed.

667   The mineralization of OM in the sediment leads to a build-up of NH_4^+ in the sediment pore-
668   water resulting in the benthic efflux of NH_4^+ (Herbert, 1999; Schulz, 2006). The absence of a
669   significant change in the NH_4^+ pore-water profiles during the temporal study carried out in 2015
670   agrees with the lack of temporal variations in diffusive NH_4^+ fluxes, implying that a large part of
671   deposited OM is decomposed at the sediment surface before integrating the sediment column, as
672   suggested by Rabouille et al. (2021) for the Louisiana shelf. Relatively low diffusive NH_4^+ fluxes
673   compared to the measured fluxes confirms that significant NH_4^+ production took place through
674   aerobic OM mineralization at the SWI in contact with the bottom water. This pattern is consistent
675   with the relatively low C_{org} values (1.6% DW) of the VB sediments, compared to other eutrophic
676   coastal ecosystems, such as Kiel Bight (3.0-5.0% DW; Balzer et al., 1986) and Aarhus Bay (2.5-
677   3.8% DW; Dale et al., 2008).

678   In shallow coastal environments, sediment resuspension due to tides, swells and wind may
679   influence benthic fluxes of dissolved substances (Boynton et al., 2018). The absence of a
680   significant difference between benthic flux measurement values during spring and neap tides
681   suggests the minor influence of tidal cycles on SWI DIN and DON exchanges. Sanford et al.
682   (1991) reported that tides had a minor influence on sediment resuspension in the Chesapeake Bay
683   compared to strong wind episodes. In the VB, large sediment resuspension occurs generally in
684   winter in relation with strong hydrodynamic conditions, e.g., during winter storms where several
685   centimeters of sediment can be resuspended (Goubert et al., 2010). This is reflected by the constant
686   depth profiles of granulometry, C_{org} and TN (Bunke et al., 2019). Moreover, sediment resuspension
687   in the VB is often accompanied by high turbidity values in the bottom waters (>100 NTU, Retho
688   et al. 2020). Nevertheless, turbidity values measured at the ND station during the study period
689   remained low (<10 NTU). The persistence of the concentration gradient for the dissolved
690   compounds in the pore-water suggests that sediments have not undergone strong resuspension
691   during the study period. In addition, we did not find any significant correlation between bottom
692   water turbidity and benthic N transformation rates or N fluxes (Table S9).

693   Different types of OM can be deposited in the VB sediments from external sources. The
694   riverine input of particulate OM is limited due to efficient recycling in the Loire estuary (Relexans
695   et al., 1988) and the presence of a dam in the Vilaine estuary (Traini et al., 2015). Phytoplankton
696   from oceanic waters may not be substantial due to lower biomass than in the VB (Ratmaya et al.,
697   2019). The positive correlation between the measured NH_4^+ fluxes and sediment Chl *a*

698   concentrations in the VB (Fig. S10a) indicates that benthic NH_4^+ fluxes are dependent on the

699   sedimentation of the phytoplankton (Cowan and Boynton, 1996). This has been shown previously

700   for different coastal ecosystems such as Aarhus Bay (Jensen et al., 1990) and San Francisco Bay

701   (Caffrey, 1995). The observations in the water column and sediment surface, together with the

702   BSi, C_{org} and TN content in the top first five cm of the sediment confirm that diatom blooms are

703   the main source of OM to the VB sediments, with the north-western part as the favored deposition

704   area (Le Bris and Glémarec, 1996; Ehrhold, 2014).

705   Diatom blooms in the VB are predominantly driven by nutrient inputs associated with

706   floods from the Loire and Vilaine rivers (Figs. 2, S2). After blooms appear, the deposited diatom-

707   derived OM is mostly mineralized aerobically at the SWI within 2-3 weeks and recycled directly

708   to the water column as dissolved inorganic (NH_4^+) and organic N (Fig. 9a). When blooms are

709   absent, benthic dissolved N fluxes decrease and may be supported essentially by a diffusion from

710   the deeper sediment layer, especially for DIN (Fig. 9b). For both situations, the diffusion of DON

711   from a deeper sediment layer is very low, implying that DON is instead gradually mineralized to

712   NH_4^+ in the pore-water. In addition, decomposition of the deposited phytoplanktonic material can

713   rapidly consume O_2 at the sediment surface (within hours to several days) and can be followed by

714   O_2 depletion in the bottom water, especially during summer. This pattern may also be valid for

715   other coastal ecosystems with similar characteristics as the VB, as was reported in oxic sediments

716   from the North Sea (De Borger et al., 2021) and in the seasonally hypoxic sediments of the northern

717   Gulf of Mexico (Rabouille et al., 2021). The overall results lead to conclude that temporal and

718   spatial variations of the benthic DIN and DON fluxes in the VB depend predominantly on the

719   sedimentation of the diatom blooms rather than on the composition of the sediment column itself.

720   *4.5.   Ecological implication of benthic DIN fluxes compared to riverine inputs*

721   DIN constitute the limiting nutrient of eutrophication during summer in the VB (Ratmaya

722   et al., 2019). One can wonder how sedimentary and riverine sources contribute to summer DIN

723   budget of the VB. These DIN flux data can be used to give a rough estimate of the role played by

724   sediments in this budget for two different summer scenarios, low water and flood situations in

725   2015 and 2016 respectively. Benthic DIN fluxes measured in summer 2015 (June-September) at

726   the ND station brings around 225 t N to the VB water column, when extrapolated to the surface of

727   the muddy area (~40% of the total area, 220 km^2, Ehrhold, 2014). For the same period, the Loire

728   delivers around 820 t N by applying a dilution of 20-fold at its outlet, while the Vilaine carried up

729   to 1,120 t N to the VB water column. For this low water scenario, benthic DIN inputs therefore

730   represent around 15% of the riverine inputs. For the summer flood scenario in 2016, benthic DIN

731 inputs (~360 t N) represent up to 30% of DIN riverine inputs, estimated for 430 t N from the
732 Vilaine and 930 t N from the Loire by applying the same dilution. This higher contribution of
733 benthic DIN source during the summer flood scenario is related to the higher benthic DIN
734 recycling due to higher OM inputs to the sediment surface compared to low water scenario. Despite
735 its uncertainty, this rough estimate suggest that sediments constitute a non-negligible source of
736 DIN to the VB water column, aggravating the effect of riverine DIN inputs. The use of a 3D
737 ecological model (Ménesguen et al., 2019), that takes hydrodynamics into account is required to
738 better estimate the contribution of each DIN source to the VB water column.

5.   Conclusion and perspectives

740   The cross-interpretation of the field observations, laboratory measurements and modeling
741 approach indicate that OM inputs from diatom blooms are the key factor controlling benthic N
742 cycling in the VB. The rapid decomposition of the deposited diatom material at the SWI may be
743 followed by the depletion of the O_2 concentration in the bottom water, especially when blooms
744 occur in summer. Using the same fixed model parameters, the RTM can be used to interpret both
745 the time series and the spatial dataset for the benthic N cycle as a function of the OM deposition
746 rate and the sedimentary environments. The dynamics of the DON fluxes still need to be
747 investigated before they can be integrated into the RTM. The interpolation of benthic DIN flux
748 measurement to the surface area of the VB, suggests that sediments represent a non-negligible
749 source of DIN compared to riverine inputs.

750   In order to obtain a seasonal and spatial description of the biogeochemical processes in
751 both the sediment and water column, the results presented in this study must be integrated into a
752 3D ecological model (see Ménesguen et al., 2019 for ECOMARS3D model). Our key results
753 provide the dataset to parameterize the sediment biogeochemical processes (e.g., nutrient
754 transformation, elimination, and/or immobilization) in the ecological model. This integration will
755 improve the ecological model in order to more accurately predict the sequence of river floods,
756 phytoplankton blooms, sedimentation, benthic mineralization and bottom water hypoxia in the
757 VB.

774   **References**

775   Ait Ballagh, F.E., Rabouille, C., Andrieux-Loyer, F., Soetaert, K., Lansard, B., Bombled, B.,
776   Monvoisin, G., Elkalay, K., Khalil, K., 2021. Spatial variability of organic matter and
777   phosphorus cycling in Rhône River prodelta sediments (NW Mediterranean Sea, France):
778   a model-data approach. Estuar. Coast. https://dx.doi.org/10.1007/s12237-020-00889-9.

779   Akbarzadeh, Z., Laverman, A.M., Rezanezhad, F., Raimonet, M., Viollier, E., Shafei, B., Van
780   Cappellen, P., 2018. Benthic nitrite exchanges in the Seine River (France): An early
781   diagenetic modeling analysis. Sci. Total Environ. 628-629, 580-593.
782   https://dx.doi.org/10.1016/j.scitotenv.2018.01.319.

783   Alkhatib, M., del Giorgio, P.A., Gelinas, Y., Lehmann, M.F., 2013. Benthic fluxes of dissolved
784   organic nitrogen in the lower St. Lawrence estuary and implications for selective organic
785   matter degradation. Biogeosciences 10, 7609-7622. https://dx.doi.org/10.5194/bg-10-
786   7609-2013.

787   Aller, R.C., Aller, J.Y., 1998. The effect of biogenic irrigation intensity and solute exchange on
788   diagenetic reaction rates in marine sediments. J. Mar. Res. 56, 905-936.
789   https://dx.doi.org/10.1357/002224098321667413.

790   Alperin, M.J., Martens, C.S., Albert, D.B., Suayah, I.B., Benninger, L.K., Blair, N.E., Jahnke,
791   R.A., 1999. Benthic fluxes and porewater concentration profiles of dissolved organic
792   carbon in sediments from the North Carolina continental slope. Geochim. Cosmochim. Ac.
793   63, 427-448. https://dx.doi.org/10.1016/s0016-7037(99)00032-0.

794   Aminot, A., Kérouel, R., 2004. Hydrologie des écosystèmes marins: paramètres et analyses (in
795   French). Éditions Ifremer, Plouzané, France, p. 336.

796   Aminot, A., Kérouel, R., 2007. Dosage automatique des nutriments dans les eaux marines:
797   méthodes en flux continu (in French). Éditions Ifremer, Plouzané, France, p. 188.

798   Arndt, S., Jørgensen, B.B., LaRowe, D.E., Middelburg, J.J., Pancost, R.D., Regnier, P., 2013.
799   Quantifying the degradation of organic matter in marine sediments: A review and
800   synthesis. Earth-Sci. Rev. 123, 53-86. https://dx.doi.org/10.1016/j.earscirev.2013.02.008.

801   Balzer, W., Pollehne, F., Erlenkeuser, H., 1986. Cycling of Organic Carbon in a Coastal Marine
802   System. Springer New York, New York, NY, pp. 325-330. https://dx.doi.org/10.1007/978-
803   1-4612-4932-0_27.

804   Banta, G.T., Giblin, A.E., Hobbie, J.E., Tucker, J., 1995. Benthic respiration and nitrogen release
805   in Buzzards Bay, Massachusetts. J. Mar. Res. 53, 107-135.
806   https://dx.doi.org/10.1357/0022240953213287.

807　Belin, C., Soudant, D., Amzil, Z., 2020. Three decades of data on phytoplankton and phycotoxins
808　　　　on the French coast: Lessons from REPHY and REPHYTOX. Harmful Algae 101733.
809　　　　https://dx.doi.org/10.1016/j.hal.2019.101733.
810　Bianchi, M., Bonin, P., Feliatra, F., 1994. Bacterial nitrification and denitrification rates in the
811　　　　Rhone river plume (northwestern Mediterranean-Sea). Mar. Ecol. Prog. Ser. 103, 197-202.
812　　　　https://dx.doi.org/10.3354/meps103197.
813　Blackburn, T.H., Henriksen, K., 1983. Nitrogen cycling in different types of sediments from
814　　　　Danish　　　　waters[1].　　　Limnol.　　Oceanogr.　　28,　　　477-493.
815　　　　https://dx.doi.org/10.4319/lo.1983.28.3.0477.
816　Bohlen, L., Dale, A.W., Sommer, S., Mosch, T., Hensen, C., Noffke, A., Scholz, F., Wallmann,
817　　　　K., 2011. Benthic nitrogen cycling traversing the Peruvian oxygen minimum zone.
818　　　　Geochim. Cosmochim. Ac. 75, 6094-6111. https://dx.doi.org/10.1016/j.gca.2011.08.010.
819　Boudreau, B.P., 1997. Diagenetic Models and Their Implementation : Modelling Transport and
820　　　　Reactions in Aquatic Sediments. Springer-Verlag, Berlin.
821　Boynton, W.R., Ceballos, M.A.C., Bailey, E.M., Hodgkins, C.L.S., Humphrey, J.L., Testa, J.M.,
822　　　　2018. Oxygen and nutrient exchanges at the sediment-water interface: A global synthesis
823　　　　and　critique　of　estuarine　and　coastal　data.　Estuar.　Coast.　41,　301-333.
824　　　　https://dx.doi.org/10.1007/s12237-017-0275-5.
825　Brigolin, D., Pastres, R., Nickell, T.D., Cromey, C.J., Aguilera, D.R., Regnier, P., 2009. Modelling
826　　　　the impact of aquaculture on early diagenetic processes in sea loch sediments. Mar. Ecol.
827　　　　Prog. Ser. 388, 63-80. https://dx.doi.org/10.3354/meps08072.
828　Bunke, D., Leipe, T., Moros, M., Morys, C., Tauber, F., Virtasalo, J.J., Forster, S., Arz, H.W.,
829　　　　2019. Natural and anthropogenic sediment mixing processes in the South-Western Baltic
830　　　　Sea. Front. Mar. Sci. 6, https://dx.doi.org/10.3389/fmars.2019.00677.
831　Burdige, D.J., 2001. Dissolved organic matter in Chesapeake Bay sediment pore waters. Org.
832　　　　Geochem. 32, 487-505. https://dx.doi.org/10.1016/s0146-6380(00)00191-1.
833　Burdige, D.J., Alperin, M.J., Homstead, J., Martens, C.S., 1992. The role of benthic fluxes of
834　　　　dissolved organic carbon in oceanic and sedimentary carbon cycling. Geophys. Res. Lett.
835　　　　19, 1851-1854. https://dx.doi.org/10.1029/92gl02159.
836　Burdige, D.J., Komada, T., 2002. Sediment Pore Waters In: Hansell, D.A., Carlson, C.A. (Eds.),
837　　　　Biogeochemistry of Marine Dissolved Organic Matter (second edition). Academic Press,
838　　　　San Diego, pp. 535-577. https://dx.doi.org/10.1016/B978-012323841-2/50015-4.
839　Burdige, D.J., Komada, T., Magen, C., Chanton, J.P., 2016. Modeling studies of dissolved organic
840　　　　matter cycling in Santa Barbara Basin (CA, USA) sediments. Geochim. Cosmochim. Ac.
841　　　　195, 100-119. https://dx.doi.org/10.1016/j.gca.2016.09.007.
842　Burdige, D.J., Zheng, S., 1998. The biogeochemical cycling of dissolved organic nitrogen in
843　　　　estuarine　　　　sediments.　　　Limnol.　　Oceanogr.　　43,　　　1796-1813.
844　　　　https://dx.doi.org/10.4319/lo.1998.43.8.1796.
845　Caffrey, J.M., 1995. Spatial and seasonal patterns in sediment nitrogen remineralization and
846　　　　ammonium concentrations in San Francisco Bay, California. Estuaries 18, 219-233.
847　　　　https://dx.doi.org/10.2307/1352632.
848　Canavan, R.W., Laverman, A.M., Slomp, C.P., 2007. Modeling nitrogen cycling in a coastal fresh
849　　　　water sediment. Hydrobiologia 584, 27-36. https://dx.doi.org/10.1007/s10750-007-0583-
850　　　　z.
851　Canavan, R.W., Slomp, C.P., Jourabchi, P., Van Cappellen, P., Laverman, A.M., van den Berg,
852　　　　G.A., 2006. Organic matter mineralization in sediment of a coastal freshwater lake and
853　　　　response　to　salinization.　Geochim.　Cosmochim.　Ac.　70,　2836-2855.
854　　　　https://dx.doi.org/10.1016/j.gca.2006.03.012.
855　Canfield, D.E., 1993. Organic Matter Oxidation in Marine Sediments. Springer Berlin Heidelberg,
856　　　　Berlin, Heidelberg, pp. 333-363. https://dx.doi.org/10.1007/978-3-642-76064-8_14.

857 Carstensen, J., Klais, R., Cloern, J.E., 2015. Phytoplankton blooms in estuarine and coastal waters:
858   Seasonal patterns and key species. Estuar. Coast. Shelf Sci. 162, 98-109.
859   https://dx.doi.org/10.1016/j.ecss.2015.05.005.
860 Cauwet, G., 1975. Optimisation d'une technique de dosage du carbone organique des sédiments.
861   Chem. Geol. 16, 59-63. https://dx.doi.org/10.1016/0009-2541(75)90091-1.
862 Chapelle, A., 1991. Modélisation d'un écosystème marin côtier soumis à l'eutrophisation : la Baie
863   de Vilaine (Sud Bretagne). Etude du phytoplancton et du bilan en oxygène (in French).
864   Université Paris VI, p. 214.
865 Cloern, J.E., 2001. Our evolving conceptual model of the coastal eutrophication problem. Mar.
866   Ecol. Prog. Ser. 210, 223-253. https://dx.doi.org/10.3354/meps210223.
867 Couture, R.M., Shafei, B., Van Cappellen, P., Tessier, A., Gobeil, C., 2010. Non-steady state
868   modeling of arsenic diagenesis in lake sediments. Environ. Sci. Technol. 44, 197-203.
869   https://dx.doi.org/10.1021/es902077q.
870 Cowan, J.L.W., Boynton, W.R., 1996. Sediment-water oxygen and nutrient exchanges along the
871   longitudinal axis of Chesapeake Bay: Seasonal patterns, controlling factors and ecological
872   significance. Estuaries 19, 562-580. https://dx.doi.org/10.2307/1352518.
873 Cowie, G.L., Hedges, J.I., Calvert, S.E., 1992. Sources and relative reactivities of amino acids,
874   neutral sugars, and lignin in an intermittently anoxic marine environment. Geochim.
875   Cosmochim. Ac. 56, 1963-1978. https://dx.doi.org/10.1016/0016-7037(92)90323-b.
876 Dale, A.W., Aguilera, D.R., Regnier, P., Fossing, H., Knab, N.J., Jørgensen, B.B., 2008. Seasonal
877   dynamics of the depth and rate of anaerobic oxidation of methane in Aarhus Bay
878   (Denmark) sediments. J. Mar. Res. 66, 127-155.
879   https://dx.doi.org/10.1357/002224008784815775.
880 Dale, A.W., Sommer, S., Bohlen, L., Treude, T., Bertics, V.J., Bange, H.W., Pfannkuche, O.,
881   Schorp, T., Mattsdotter, M., Wallmann, K., 2011. Rates and regulation of nitrogen cycling
882   in seasonally hypoxic sediments during winter (Boknis Eck, SW Baltic Sea): Sensitivity to
883   environmental variables. Estuar. Coast. Shelf Sci. 95, 14-28.
884   https://dx.doi.org/10.1016/j.ecss.2011.05.016.
885 Dalsgaard, T., Nielsen, L.P., Brotas, V., Viaroli, P., Underwood, G., Nedwell, D.B., Sundbäck, K.,
886   Rysgaard, S., Miles, A., Bartoli, M., Dong, L., Thornton, D.C.O., Ottosen, L.D.M.,
887   Castaldelli, G., Risgaard-Petersen, N., 2000. Protocol handbook for NICE: nitrogen
888   cycling in estuaries: a project under the EU research programme Marine Science and
889   Technology (MAST III). National Environmental Research Institute, Silkeborg, Denmark,
890   p. 64.
891 Dalsgaard, T., Thamdrup, B., Canfield, D.E., 2005. Anaerobic ammonium oxidation (anammox)
892   in the marine environment. Res. Microbiol. 156, 457-464.
893   https://dx.doi.org/10.1016/j.resmic.2005.01.011.
894 De Borger, E., Braeckman, U., Soetaert, K., 2021. Rapid organic matter cycling in North Sea
895   sediments. Cont. Shelf Res. 214, 104327. https://dx.doi.org/10.1016/j.csr.2020.104327.
896 DeMaster, D.J., 1981. The supply and accumulation of silica in the marine environment. Geochim.
897   Cosmochim. Ac. 45, 1715-1732. https://dx.doi.org/10.1016/0016-7037(81)90006-5.
898 Devol, A.H., 2015. Denitrification, anammox, and N_2 production in marine sediments. Ann. Rev.
899   Mar. Sci. 7, 403-423. https://dx.doi.org/10.1146/annurev-marine-010213-135040.
900 Ehrhold, A., 2014. Cartes sédimentologiques de Bretagne Sud : Entre baie de Vilaine et archipel
901   de Glénan (in French). QUAE, Versailles, p. 80.
902 Ehrhold, A., Blanchet, A., Hamon, D., Gaffet, J.-D., Augris, C., Duval, F., 2008. Approche
903   sectorielle subtidale : Identification et caractérisation des habitats benthiques du secteur
904   Vilaine (Réseau de surveillance benthique - Région Bretagne).
905   RST/IFREMER/DYNECO/EB/08-03/REBENT, p. 45.
906   https://archimer.ifremer.fr/doc/00000/2301/.
907 Eyre, B.D., Ferguson, A.J.P., 2002. Comparison of carbon production and decomposition, benthic
908   nutrient fluxes and denitrification in seagrass, phytoplankton, benthic microalgae- and

909   macroalgae-dominated warm-temperate Australian lagoons. Mar. Ecol. Prog. Ser. 229, 43-
910   59. https://dx.doi.org/10.3354/meps229043.

911 Fisher, T.R., Carlson, P.R., Barber, R.T., 1982. Sediment nutrient regeneration in three North
912   Carolina estuaries. Estuar. Coast. Shelf Sci. 14, 101-116. https://dx.doi.org/10.1016/s0302-
913   3524(82)80069-8.

914 Follum, O.A., Gray, J.S., 1987. Nitrogenous excretion by the sediment-living bivalve Nucula
915   tenuis from the Oslofjord, Norway. Mar. Biol. 96, 355-358.
916   https://dx.doi.org/10.1007/bf00412517.

917 Gardner, W.S., Briones, E.E., Kaegi, E.C., Rowe, G.T., 1993. Ammonium excretion by benthic
918   invertebrates and sediment-water nitrogen flux in the Gulf of Mexico near the Mississippi
919   River outflow. Estuaries 16, 799. https://dx.doi.org/10.2307/1352438.

920 Giblin, A.E., Tobias, C.R., Song, B., Weston, N., Banta, G.T., Rivera-Monroy, V.H., 2013. The
921   importance of dissimilatory nitrate reduction to ammonium (DNRA) in the nitrogen cycle
922   of coastal ecosystems. Oceanography 26, 124-131.
923   https://dx.doi.org/10.5670/oceanog.2013.54.

924 Gilbert, F., Souchu, P., Bianchi, M., Bonin, P., 1997. Influence of shellfish farming activities on
925   nitrification, nitrate reduction to ammonium and denitrification at the water-sediment
926   interface of the Thau lagoon, France. Mar. Ecol. Prog. Ser. 151, 143-153.
927   https://dx.doi.org/10.3354/meps151143.

928 Glud, R.N., 2008. Oxygen dynamics of marine sediments. Mar. Biol. Res. 4, 243-289.
929   https://dx.doi.org/10.1080/17451000801888726.

930 Glud, R.N., Gundersen, J.K., Jørgensen, B.B., Revsbech, N.P., Schulz, H.D., 1994. Diffusive and
931   total oxygen uptake of deep-sea sediments in the eastern South Atlantic Ocean: in situ and
932   laboratory measurements. Deep-Sea Res. Pt I 41, 1767-1788.
933   https://dx.doi.org/10.1016/0967-0637(94)90072-8.

934 Gohin, F., 2011. Annual cycles of chlorophyll-*a*, non-algal suspended particulate matter, and
935   turbidity observed from space and in-situ in coastal waters. Ocean Sci. 7, 705-732.
936   https://dx.doi.org/10.5194/os-7-705-2011.

937 Goubert, E., Frenod, E., Peeters, P., Thuillier, P., Vested, H.J., Bernard, N., 2010. The use of
938   altimetric data (Altus) in the characterization of hydrodynamic climates controlling
939   hydrosedimentary processes of intertidal mudflat: the Vilaine estuary case (Brittany,
940   France). Revue Paralia 3, 6.17-16.31. https://dx.doi.org/10.5150/revue-
941   paralia.2010.0066.1-6.15.

942 Gray, J.S., Wu, R.S., Or, Y.Y., 2002. Effects of hypoxia and organic enrichment on the coastal
943   marine environment. Mar. Ecol. Prog. Ser. 238, 249-279.
944   https://dx.doi.org/10.3354/meps238249.

945 Guillaud, J.-F., Aminot, A., Delmas, D., Gohin, F., Lunven, M., Labry, C., Herbland, A., 2008.
946   Seasonal variation of riverine nutrient inputs in the northern Bay of Biscay (France), and
947   patterns of marine phytoplankton response. J. Marine Syst. 72, 309-319.
948   https://dx.doi.org/10.1016/j.jmarsys.2007.03.010.

949 Gürevin, C., Erturk, A., Albay, M., 2017. Predicting the effects of sediment based internal nutrient
950   loads on eutrophication in Küçükçekmece Lagoon for rehabilitation planning. Int. J.
951   Sediment Res. 32, 527-554. https://dx.doi.org/10.1016/j.ijsrc.2016.08.002.

952 Hansen, L.S., Blackburn, T.H., 1992. Effect of algal bloom deposition on sediment respiration and
953   fluxes. Mar. Biol. 112, 147-152. https://dx.doi.org/10.1007/bf00349738.

954 Hensen, C., Landenberger, H., Zabel, M., Schulz, H.D., 1998. Quantification of diffusive benthic
955   fluxes of nitrate, phosphate, and silicate in the southern Atlantic Ocean. Global
956   Biogeochem. Cy. 12, 193-210. https://dx.doi.org/10.1029/97gb02731.

957 Herbert, R.A., 1999. Nitrogen cycling in coastal marine ecosystems. FEMS Microbiol. Rev. 23,
958   563-590. https://dx.doi.org/10.1111/j.1574-6976.1999.tb00414.x.

959 Hulth, S., Aller, R.C., Canfield, D.E., Dalsgaard, T., Engstrom, P., Gilbert, F., Sundback, K.,
960   Thamdrup, B., 2005. Nitrogen removal in marine environments: recent findings and future

28

961   research   challenges.   Mar.   Chem.   94,   125-145.
962   https://dx.doi.org/10.1016/j.marchem.2004.07.013.

963 Ifremer, L.E.R.M.P.d.L., 2015. Qualité du Milieu Marin Littoral - Bulletin de la surveillance 2014.
964   Département du Morbihan (in French). ODE/LITTORAL/LER-MPL/15-06, p. 129.
965   https://archimer.ifremer.fr/doc/00311/42183/.

966 Jäntti, H., Stange, F., Leskinen, E., Hietanen, S., 2011. Seasonal variation in nitrification and
967   nitrate-reduction pathways in coastal sediments in the Gulf of Finland, Baltic Sea. Aquat.
968   Microb. Ecol. 63, 171-181. https://dx.doi.org/10.3354/ame01492.

969 Jensen, M.H., Lomstein, E., Sørensen, J., 1990. Benthic NH_4^+ and NO_3^- flux following
970   sedimentation of a spring phytoplankton bloom in Aarhus Bight, Denmark. Mar. Ecol.
971   Prog. Ser. 61, 87-96. https://dx.doi.org/10.3354/meps061087.

972 Jørgensen, B.B., Revsbech, N.P., 1985. Diffusive boundary layers and the oxygen uptake of
973   sediments   and   detritus1.   Limnol.   Oceanogr.   30,   111-122.
974   https://dx.doi.org/10.4319/lo.1985.30.1.0111.

975 Jorgensen, K.S., Sorensen, J., 1988. Two annual maxima of nitrate reduction and denitrification
976   in estuarine sediment (Norsminde-Fjord, Denmark). Mar. Ecol. Prog. Ser. 48, 147-154.
977   https://dx.doi.org/10.3354/meps048147.

978 Kemp, W.M., Boynton, W.R., Adolf, J.E., Boesch, D.F., Boicourt, W.C., Brush, G., Cornwell,
979   J.C., Fisher, T.R., Glibert, P.M., Hagy, J.D., Harding, L.W., Houde, E.D., Kimmel, D.G.,
980   Miller, W.D., Newell, R.I.E., Roman, M.R., Smith, E.M., Stevenson, J.C., 2005.
981   Eutrophication of Chesapeake Bay: historical trends and ecological interactions. Mar. Ecol.
982   Prog. Ser. 303, 1-29. https://dx.doi.org/10.3354/meps303001.

983 Kemp, W.M., Sampou, P., Caffrey, J., Mayer, M., Henriksen, K., Boynton, W.R., 1990.
984   Ammonium recycling versus denitrification in Chesapeake Bay sediments. Limnol.
985   Oceanogr. 35, 1545-1563.

986 Khalil, K., Laverman, A.M., Raimonet, M., Rabouille, C., 2018. Importance of nitrate reduction
987   in benthic carbon mineralization in two eutrophic estuaries: Modeling, observations and
988   laboratory   experiments.   Mar.   Chem.   199,   24-36.
989   https://dx.doi.org/10.1016/j.marchem.2018.01.004.

990 Kitidis, V., Tait, K., Nunes, J., Brown, I., Woodward, E.M.S., Harris, C., Sabadel, A.J.M., Sivyer,
991   D.B., Silburn, B., Kröger, S., 2017. Seasonal benthic nitrogen cycling in a temperate shelf
992   sea: the Celtic Sea. Biogeochemistry 135, 103-119. https://dx.doi.org/10.1007/s10533-
993   017-0311-3.

994 Komada, T., Burdige, D.J., Crispo, S.M., Druffel, E.R.M., Griffin, S., Johnson, L., Le, D., 2013.
995   Dissolved organic carbon dynamics in anaerobic sediments of the Santa Monica Basin.
996   Geochim. Cosmochim. Ac. 110, 253-273. https://dx.doi.org/10.1016/j.gca.2013.02.017.

997 Lansard, B., Rabouille, C., Denis, L., Grenz, C., 2008. In situ oxygen uptake rates by coastal
998   sediments under the influence of the Rhône River (NW Mediterranean Sea). Cont. Shelf
999   Res. 28, 1501-1510. https://dx.doi.org/10.1016/j.csr.2007.10.010.

1000 Laverman, A.M., Pallud, C., Abell, J., Van Cappellen, P., 2012. Comparative survey of potential
1001   nitrate and sulfate reduction rates in aquatic sediments. Geochim. Cosmochim. Ac. 77,
1002   474-488. https://dx.doi.org/10.1016/j.gca.2011.10.033.

1003 Laverman, A.M., Van Cappellen, P., van Rotterdam-Los, D., Pallud, C., Abell, J., 2006. Potential
1004   rates and pathways of microbial nitrate reduction in coastal sediments. FEMS Microbiol.
1005   Ecol. 58, 179-192. https://dx.doi.org/10.1111/j.1574-6941.2006.00155.x.

1006 Lazure, P., Jegou, A.-M., 1998. 3D modelling of seasonal evolution of Loire and Gironde plumes
1007   on   Biscay   Bay   continental   shelf.   Oceanol.   Acta   21,   165-177.
1008   https://dx.doi.org/10.1016/s0399-1784(98)80006-6.

1009 Le Bris, H., Glémarec, M., 1996. Marine and brackish ecosystems of south Brittany (Lorient and
1010   Vilaine Bays) with particular reference to the effect of the turbidity maxima. Estuar. Coast.
1011   Shelf Sci. 42, 737-753. https://dx.doi.org/10.1006/ecss.1996.0047.

1012 Le Moal, M., Gascuel-Odoux, C., Menesguen, A., Souchon, Y., Etrillard, C., Levain, A., Moatar,
1013   F., Pannard, A., Souchu, P., Lefebvre, A., Pinay, G., 2019. Eutrophication: A new wine in
1014   an old bottle? Sci. Total Environ. 651, 1-11.
1015   https://dx.doi.org/10.1016/j.scitotenv.2018.09.139.
1016 Lorenzen, C.J., 1967. Determination of chlorophyll and pheo-pigments: spectrophotometric
1017   equations. Limnol. Oceanogr. 12, 343-346. https://dx.doi.org/10.2307/2833053.
1018 Mangan, S., Lohrer, A.M., Thrush, S.F., Pilditch, C.A., 2020. Water column turbidity not sediment
1019   nutrient enrichment moderates microphytobenthic primary production. J. Mar. Sci. Eng. 8,
1020   732. https://dx.doi.org/10.3390/jmse8100732.
1021 Ménesguen, A., Dussauze, M., Dumas, F., 2018. Designing optimal scenarios of nutrient loading
1022   reduction in a WFD/MSFD perspective by using passive tracers in a biogeochemical-3D
1023   model of the English Channel/Bay of Biscay area. Ocean Coast. Manage. 163, 37-53.
1024   https://dx.doi.org/10.1016/j.ocecoaman.2018.06.005.
1025 Ménesguen, A., Dussauze, M., Dumas, F., Thouvenin, B., Garnier, V., Lecornu, F., Répécaud, M.,
1026   2019. Ecological model of the Bay of Biscay and English Channel shelf for environmental
1027   status assessment part 1: Nutrients, phytoplankton and oxygen. Ocean Model. 133, 56-78.
1028   https://dx.doi.org/10.1016/j.ocemod.2018.11.002.
1029 Middelburg, J.J., Levin, L.A., 2009. Coastal hypoxia and sediment biogeochemistry.
1030   Biogeosciences 6, 1273-1293. https://dx.doi.org/10.5194/bg-6-1273-2009.
1031 Middelburg, J.J., Soetaert, K., Herman, P.M.J., Heip, C.H.R., 1996. Denitrification in marine
1032   sediments: A model study. Global Biogeochem. Cy. 10, 661-673.
1033   https://dx.doi.org/10.1029/96gb02562.
1034 Miller, D.C., Geider, R.J., MacIntyre, H.L., 1996. Microphytobenthos: The ecological role of the
1035   "secret garden" of unvegetated, shallow-water marine habitats. Ii. Role in sediment
1036   stability and shallow-water food webs. Estuaries 19, 202.
1037   https://dx.doi.org/10.2307/1352225.
1038 Mogg, A.O.M., Attard, K.M., Stahl, H., Brand, T., Turnewitsch, R., Sayer, M.D.J., 2017. The
1039   influence of coring method on the preservation of sedimentary and biogeochemical
1040   features when sampling soft-bottom, shallow coastal environments. Limnol. Oceanogr.
1041   Methods 15, 905-915. https://dx.doi.org/10.1002/lom3.10211.
1042 Mordy, C.W., Eisner, L.B., Proctor, P., Stabeno, P., Devol, A.H., Shull, D.H., Napp, J.M.,
1043   Whitledge, T., 2010. Temporary uncoupling of the marine nitrogen cycle: Accumulation
1044   of nitrite on the Bering Sea shelf. Mar. Chem. 121, 157-166.
1045   https://dx.doi.org/10.1016/j.marchem.2010.04.004.
1046 Paerl, H.W., 2018. Why does N-limitation persist in the world's marine waters? Mar. Chem. 206,
1047   1-6. https://dx.doi.org/10.1016/j.marchem.2018.09.001.
1048 Paraska, D.W., Hipsey, M.R., Salmon, S.U., 2014. Sediment diagenesis models: Review of
1049   approaches, challenges and opportunities. Environ. Modell. Soft. 61, 297-325.
1050   https://dx.doi.org/10.1016/j.envsoft.2014.05.011.
1051 Pastor, L., Cathalot, C., Deflandre, B., Viollier, E., Soetaert, K., Meysman, F.J.R., Ulses, C.,
1052   Metzger, E., Rabouille, C., 2011. Modeling biogeochemical processes in sediments from
1053   the Rhône River prodelta area (NW Mediterranean Sea). Biogeosciences 8, 1351-1366.
1054   https://dx.doi.org/10.5194/bg-8-1351-2011.
1055 Queiros, A.M., Birchenough, S.N., Bremner, J., Godbold, J.A., Parker, R.E., Romero-Ramirez,
1056   A., Reiss, H., Solan, M., Somerfield, P.J., Van Colen, C., Van Hoey, G., Widdicombe, S.,
1057   2013. A bioturbation classification of European marine infaunal invertebrates. Ecol. Evol.
1058   3, 3958-3985. https://dx.doi.org/10.1002/ece3.769.
1059 Rabouille, C., Lansard, B., Owings, S.M., Rabalais, N.N., Bombled, B., Metzger, E., Richirt, J.,
1060   Eitel, E.M., Boever, A.D., Beckler, J.S., Taillefert, M., 2021. Early diagenesis in the
1061   hypoxic and acidified zone of the northern Gulf of Mexico: Is organic matter recycling in
1062   sediments disconnected from the water column? Front. Mar. Sci. 8,
1063   https://dx.doi.org/10.3389/fmars.2021.604330.

Raimbault, P., Pouvesle, W., Diaz, F., Garcia, N., Sempere, R., 1999. Wet-oxidation and automated colorimetry for simultaneous determination of organic carbon, nitrogen and phosphorus dissolved in seawater. Mar. Chem. 66, 161-169. https://dx.doi.org/10.1016/S0304-4203(99)00038-9.

Ratmaya, W., 2018. Rôle des sédiments dans le cycle des nutriments et impacts sur l'eutrophisation des écosystèmes côtiers (in French). Université de Nantes, p. 212.

Ratmaya, W., Soudant, D., Salmon-Monviola, J., Plus, M., Cochennec-Laureau, N., Goubert, E., Andrieux-Loyer, F., Barillé, L., Souchu, P., 2019. Reduced phosphorus loads from the Loire and Vilaine rivers were accompanied by increasing eutrophication in the Vilaine Bay (south Brittany, France). Biogeosciences 16, 1361-1380. https://dx.doi.org/10.5194/bg-16-1361-2019.

Relexans, J.C., Meybeck, M., Billen, G., Brugeaille, M., Etcheber, H., Somville, M., 1988. Algal and microbial processes involved in particulate organic matter dynamics in the Loire estuary. Estuar. Coast. Shelf Sci. 27, 625-644. https://dx.doi.org/10.1016/0272-7714(88)90072-8.

Retho, M., 2019. Etude de la limitation de la biomasse phytoplanctonique par les nutriments dans le Mor Braz (in French). RST/LER/MPL/19.09, p. 60. https://archimer.ifremer.fr/doc/00509/62049/.

Retho, M., Quemener, L., Le Gall, C., Repecaud, M., Souchu, P., Gabellec, R., Manach, S., 2020. MOLIT Vilaine data and metadata from Coriolis Data Centre. SEANOE. https://dx.doi.org/10.17882/46529.

Risgaard-Petersen, N., 2003. Coupled nitrification-denitrification in autotrophic and heterotrophic estuarine sediments: On the influence of benthic microalgae. Limnol. Oceanogr. 48, 93-105. https://dx.doi.org/10.4319/lo.2003.48.1.0093.

Rossignol-Strick, M., 1985. A marine anoxic event on the Brittany Coast, July 1982. J. Coastal Res. 1, 11-20.

Sanford, L.P., Panageotou, W., Halka, J.P., 1991. Tidal resuspension of sediments in northern Chesapeake Bay. Mar. Geol. 97, 87-103. https://dx.doi.org/10.1016/0025-3227(91)90020-5.

Schlitzer, R., 2002. Interactive analysis and visualization of geoscience data with Ocean Data View. Comput. Geosci. 28, 1211-1218. https://dx.doi.org/10.1016/s0098-3004(02)00040-7.

Schulz, H.D., 2006. Quantification of Early Diagenesis: Dissolved Constituents in Pore Water and Signals in the Solid Phase. In: Schulz, H.D., Zabel, M. (Eds.), Marine Geochemistry. Springer Berlin Heidelberg, Berlin, Heidelberg, pp. 73-124. https://dx.doi.org/10.1007/3-540-32144-6_3.

Shull, D.H., 2019. Bioturbation☆. In: Cochran, J.K., Bokuniewicz, H.J., Yager, P.L. (Eds.), Encyclopedia of Ocean Sciences (Third Edition). Academic Press, Oxford, pp. 671-676. https://dx.doi.org/10.1016/B978-0-12-409548-9.11493-9.

Smetacek, V., 1980. Annual cycle of sedimentation in relation to plankton ecology in western Kiel Bight. Ophelia 65-76.

Smetacek, V., Zingone, A., 2013. Green and golden seaweed tides on the rise. Nature 504, 84-88. https://dx.doi.org/10.1038/nature12860.

Soetaert, K., Middelburg, J.J., 2009. Modeling eutrophication and oligotrophication of shallow-water marine systems: the importance of sediments under stratified and well-mixed conditions. In: Andersen, J.H., Conley, D.J. (Eds.), Eutrophication in Coastal Ecosystems. Springer Netherlands, pp. 239-254. https://dx.doi.org/10.1007/978-90-481-3385-7_20.

Sundbäck, K., Miles, A., Linares, F., 2006. Nitrogen dynamics in nontidal littoral sediments: Role of microphytobenthos and denitrification. Estuar. Coast. 29, 1196-1211. https://dx.doi.org/10.1007/bf02781820.

Sundbäck, K., Nilsson, P., Nilsson, C., Jönsson, B., 1996. Balance between autotrophic and heterotrophic components and processes in microbenthic communities of sandy sediments:

31

1116   A field study. Estuar. Coast. Shelf Sci. 43, 689-706.
1117   https://dx.doi.org/10.1006/ecss.1996.0097.

1118 Szymczak-Żyła, M., Kowalewska, G., Louda, J.W., 2011. Chlorophyll-a and derivatives in recent
1119   sediments as indicators of productivity and depositional conditions. Mar. Chem. 125, 39-
1120   48. https://dx.doi.org/10.1016/j.marchem.2011.02.002.

1121 Taguchi, S., 1982. Sedimentation of newly produced particulate organic matter in a subtropical
1122   inlet, Kaneohe Bay, Hawaii. Estuar. Coast. Shelf Sci. 14, 533-544.
1123   https://dx.doi.org/10.1016/s0302-3524(82)80075-3.

1124 Tessier, C., Le Hir, P., Dumas, F., Jourdin, F., 2011. Modélisation des turbidités en Bretagne Sud
1125   et validation par des mesures in situ. Eur. J. Environ. Civ. En. 12, 179-190.
1126   https://dx.doi.org/10.1080/19648189.2008.9693003.

1127 Testa, J.M., Li, Y., Lee, Y.J., Li, M., Brady, D.C., Di Toro, D.M., Kemp, W.M., Fitzpatrick, J.J.,
1128   2014. Quantifying the effects of nutrient loading on dissolved O_2 cycling and hypoxia in
1129   Chesapeake Bay using a coupled hydrodynamic–biogeochemical model. J. Marine Syst.
1130   139, 139-158. https://dx.doi.org/10.1016/j.jmarsys.2014.05.018.

1131 Thamdrup, B., Dalsgaard, T., 2002. Production of N_2 through anaerobic ammonium oxidation
1132   coupled to nitrate reduction in marine sediments. Applied and Environmental
1133   Microbiology 68, 1312-1318. https://dx.doi.org/10.1128/aem.68.3.1312-1318.2002.

1134 Torres, E., Couture, R.M., Shafei, B., Nardi, A., Ayora, C., Van Cappellen, P., 2015. Reactive
1135   transport modeling of early diagenesis in a reservoir lake affected by acid mine drainage:
1136   Trace metals, lake overturn, benthic fluxes and remediation. Chem. Geol. 419, 75-91.
1137   https://dx.doi.org/10.1016/j.chemgeo.2015.10.023.

1138 Traini, C., Proust, J.N., Menier, D., Mathew, M.J., 2015. Distinguishing natural evolution and
1139   human impact on estuarine morpho-sedimentary development: A case study from the
1140   Vilaine Estuary, France. Estuar. Coast. Shelf Sci. 163, 143-155.
1141   https://dx.doi.org/10.1016/j.ecss.2015.06.025.

1142 Turner, B.L., Matson, P.A., McCarthy, J.J., Corell, R.W., Christensen, L., Eckley, N., Hovelsrud-
1143   Broda, G.K., Kasperson, J.X., Kasperson, R.E., Luers, A., Martello, M.L., Mathiesen, S.,
1144   Naylor, R., Polsky, C., Pulsipher, A., Schiller, A., Selin, H., Tyler, N., 2003. Illustrating
1145   the coupled human-environment system for vulnerability analysis: three case studies. Proc.
1146   Natl. Acad. Sci. U S A 100, 8080-8085. https://dx.doi.org/10.1073/pnas.1231334100.

1147 Wang, Y.F., VanCappellen, P., 1996. A multicomponent reactive transport model of early
1148   diagenesis: Application to redox cycling in coastal marine sediments. Geochim.
1149   Cosmochim. Ac. 60, 2993-3014. https://dx.doi.org/10.1016/0016-7037(96)00140-8.

1150 Ward, B.B., 2008. Nitrification in Marine Systems. In: Capone, D.G., Bronk, D.A., Mulholland,
1151   M.R., Carpenter, E.J. (Eds.), Nitrogen in the Marine Environment (2nd Edition). Academic
1152   Press, San Diego, pp. 199-261.

1153 Westrich, J.T., Berner, R.A., 1984. The role of sedimentary organic matter in bacterial sulfate
1154   reduction: The *G* model tested[1]. Limnol. Oceanogr. 29, 236-249.
1155   https://dx.doi.org/10.4319/lo.1984.29.2.0236.

1156 Yamamuro, M., Koike, I., 1998. Concentrations of nitrogen in sandy sediments of a eutrophic
1157   estuarine lagoon. Hydrobiologia 386, 37-44. https://dx.doi.org/10.1023/a:1003414028040.

1158 Zhang, J., Gilbert, D., Gooday, A.J., Levin, L., Naqvi, S.W.A., Middelburg, J.J., Scranton, M.,
1159   Ekau, W., Peña, A., Dewitte, B., Oguz, T., Monteiro, P.M.S., Urban, E., Rabalais, N.N.,
1160   Ittekkot, V., Kemp, W.M., Ulloa, O., Elmgren, R., Escobar-Briones, E., Van der Plas, A.K.,
1161   2010. Natural and human-induced hypoxia and consequences for coastal areas: synthesis
1162   and future development. Biogeosciences 7, 1443-1467. https://dx.doi.org/10.5194/bg-7-
1163   1443-2010.

1164 **Figure captions**

1165 **Fig. 1** Location of the study area. The off-shore limit of the Vilaine Bay is indicated by a dashed
1166 line. The bathymetry (GEBCO bathymetry data in Ocean Data View) is displayed using the colors
1167 corresponding to the scale on the right of the graph. The sampling location of the sediment cores
1168 is indicated by red circles, the Nord Dumet monitoring station for the temporal study carried out
1169 from April to September 2015 and St. A, B, C, & D for the spatial study carried out in July 2016.
1170 The green squares correspond to the REPHY monitoring stations. The black dots are the spatial
1171 sampling points of the superficial sediments in April 2016.

1172 **Fig. 2** Variations in the salinity and river discharge (Loire and Vilaine) (a, e), temperature and
1173 dissolved O_2 (b, f), $NO_3^- + NO_2^-$ and NH_4^+ (c, g), Chl a in the water column and sediment surface
1174 (d, h), at the Nord Dumet monitoring station (St. A) in 2015 (left) and 2016 (right) from January
1175 to December. Dashed-dotted horizontal line (panels b & f): hypoxia threshold (63 µM; Middelburg
1176 and Levin, 2009; Zhang et al., 2010). Vertical lines: dates of the sediment investigations. ST and
1177 NT: spring and neap tides. Color symbols: Chl a concentration in the first top cm of the sediment
1178 ($n = 3$).

1179 **Fig. 3** Depth profiles of the organic carbon, C_{org} (a), total nitrogen, TN (b) and C:N ratios (c) for
1180 the triplicate sediment cores at the Nord Dumet monitoring station (St. A) for the temporal study
1181 from April to September 2015. No measurements were taken on April 15th.

1182 **Fig. 4** Modeled (red curves) and measured (symbols) pore-water concentration profiles of O_2 (a),
1183 NH_4^+ (b), NO_3^- (c) and NO_2^- (d) in the temporal study from April to September 2015 conducted at
1184 the Nord Dumet monitoring station (St. A). The symbols correspond to the results from the
1185 triplicate sediment cores for the nutrients and the O_2 measurements. Dashed lines: sediment-water
1186 interface (SWI).

1187 **Fig. 5** Measured and simulated NH_4^+ (a), DON (b), NO_3^- (c) and NO_2^- (d) fluxes across the SWI
1188 in the Vilaine Bay during the temporal study carried out from April to September 2015 conducted
1189 at the Nord Dumet monitoring station (St. A, left) and the spatial study carried out in July 2016
1190 (right). The error bars represent the standard error of the mean ($n = 4$). There were no model
1191 simulations for the DON fluxes.

1192 **Fig. 6** Relationship between the measured NH_4^+ fluxes and Chl a content (a), NH_4^+ and DON
1193 fluxes (b) for the temporal study carried out in 2015. The equation and the regression line were
1194 obtained from linear regression.

1195 **Fig. 7** Model sensitivity analysis showing the response of the benthic NH_4^+ fluxes during the
1196 temporal study carried out from April to September 2015 (a-f) to different scenarios of change in
1197 environmental factor-related model parameters. The response was calculated as a percentage of
1198 change in the NH_4^+ fluxes with regard to the baseline simulation (zero dashed line). The factors
1199 lying furthest from the zero dashed line are those causing the greatest change in the NH_4^+ fluxes.
1200 Anoxic: zero bottom water O_2 concentrations; BW NO_3^- = 10x [100x]: increase in the bottom
1201 water NO_3^- concentrations by 10 fold or 100 fold for August and September; OM1 2x [3x]:
1202 increase in the deposition of OM1 by 2 fold (or 3x for August); OM1 <=> OM2: inversing the
1203 proportion of OM1 and OM2; k1 OM1 = 2x: increase in the rate constant for the aerobic oxidation
1204 of OM1 by 2 fold); k1 OM1 = 1/2 x decrease in the rate constant for the aerobic oxidation of OM1
1205 by one-half; C/N OM1 = 106/16: imposed change in the C/N ratio compared to that in living
1206 phytoplankton i.e., Redfield ratio; Db = 10x: increase in the bioturbation coefficient by 10 fold; α
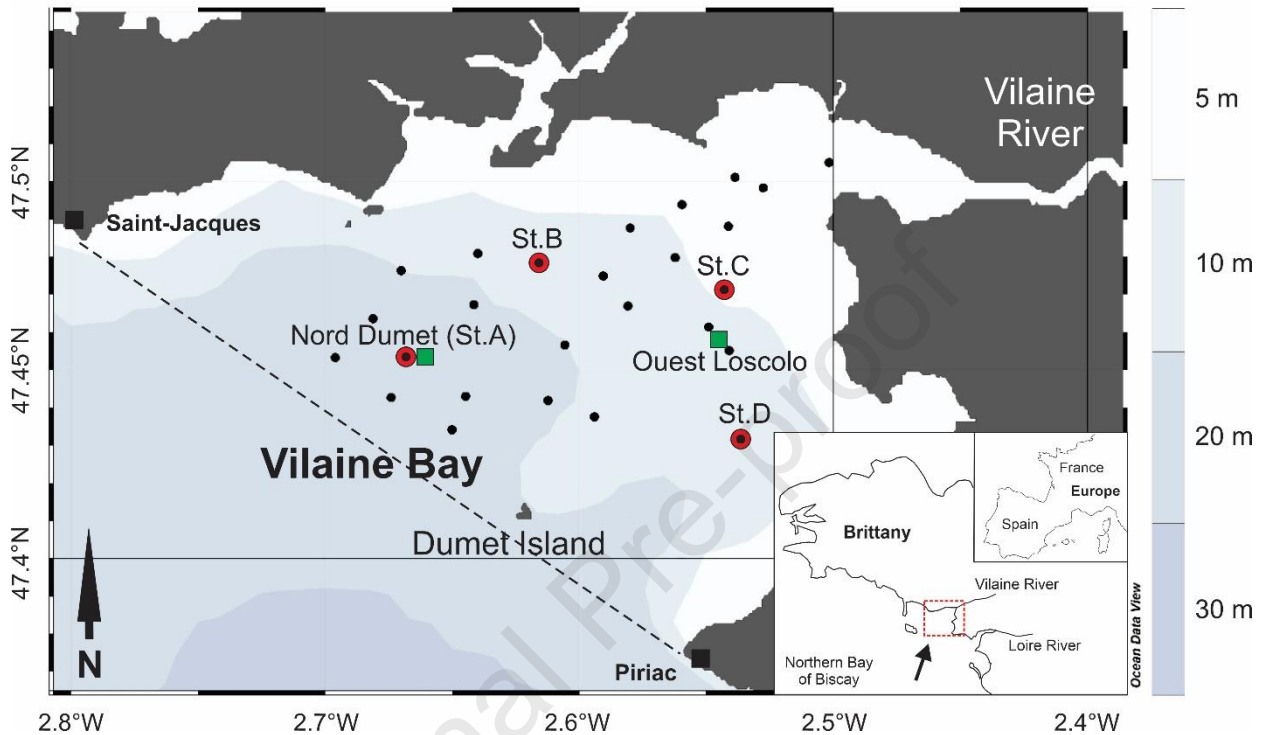1207 = 10x: increase in the bioirrigation coefficient by 10 fold.

Fig. 8 Model sensitivity analysis showing the response of the benthic NO_3^- fluxes during the temporal study carried out from April to September 2015 (a-f) to different scenarios of change in environmental factor-related model parameters. The response was calculated as a percentage of change in the NO_3^- fluxes with regard to the baseline simulation (zero dashed line). The factors lying furthest from the zero dashed line are those causing the greatest change in the NO_3^- fluxes. Anoxic: zero bottom water O_2 concentrations; BW NO_3^- = 10x [100x]: increase in the bottom water NO_3^- concentrations by 10 fold or 100 fold for August and September; OM1 2x [3x]: increase in the deposition of OM1 by 2 fold (or 3x for August); OM1 <=> OM2: inversing the proportion of OM1 and OM2; k1 OM1 = 2x: increase in the rate constant for the aerobic oxidation of OM1 by 2 fold); k1 OM1 = 1/2 x decrease in the rate constant for the aerobic oxidation of OM1 by one-half; C/N OM1 = 106/16: imposed change in the C/N ratio compared to that in living phytoplankton i.e., Redfield ratio; Db = 10x: increase in the bioturbation coefficient by 10 fold; α = 10x: increase in the bioirrigation coefficient by 10 fold.

Fig. 9 Summary diagram of the benthic N fluxes in the Vilaine Bay for two distinct situations: (a) in the presence of a phytoplankton bloom and (b) in the absence of a phytoplankton bloom, based on field observations, laboratory measurements and a modeling study. The terms OM1 and OM2 are used to distinguish between a labile and a less labile pool of organic matter input. DIN and DON stand for dissolved inorganic and organic N, respectively. The different arrow sizes indicate the magnitude of the OM input for each pool, as well as its recycling into DIN (mostly NH_4^+) and DON. The horizontal dashed lines are meant to approximately illustrate the OM turnover time for each pathway (aerobic and anaerobic), estimated from the model rate constants of OM1 and OM2 (Table S3) and the residence time of solutes (Table S6). Where the DON diffusion from pore-water is questioned, this is indicated by a question mark.

1231 **Table captions**

1232 **Table 1** Model-predicted OM decomposition rates through the different pathways for OM1 and
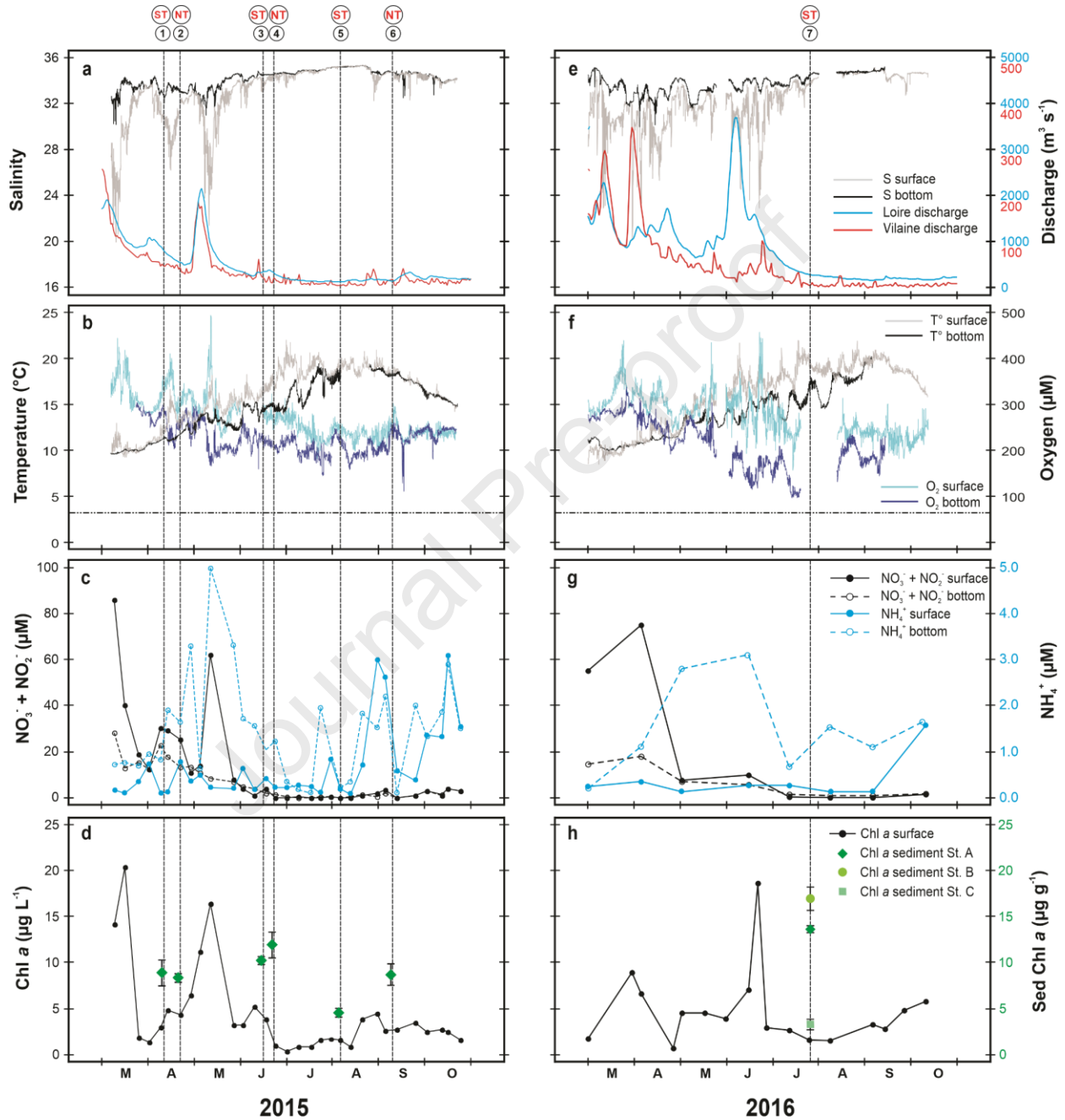1233 OM2 (in parentheses). All values are in μmol C m^{-2} h^{-1}

1234 **Table 2** Model-predicted depth-integrated N transformation rates derived from a model
1235 simulation. The measured potential nitrification step 1 and NO_3^- reduction rates are indicated in
1236 parentheses (mean $\pm$ SE). All values are in μmol N m^{-2} h^{-1}.

1237 **Fig. 1** Location of the study area. The off-shore limit of the Vilaine Bay is indicated by a dashed
1238 line. The bathymetry (GEBCO bathymetry data in Ocean Data View) is displayed using the colors
1239 corresponding to the scale on the right of the graph. The sampling location of the sediment cores
1240 is indicated by red circles, the Nord Dumet monitoring station for the temporal study carried out
1241 from April to September 2015 and St. A, B, C, & D for the spatial study carried out in July 2016.
1242 The green squares correspond to the REPHY monitoring stations. The black dots are the spatial
1243 sampling points of the superficial sediments in April 2016.

1244

1245

1246 **Fig. 2** Variations in the salinity and river discharge (Loire and Vilaine) (a, e), temperature and
1247 dissolved O_2 (b, f), $NO_3^- + NO_2^-$ and NH_4^+ (c, g), Chl *a* in the water column and sediment surface
1248 (d, h), at the Nord Dumet monitoring station (St. A) in 2015 (left) and 2016 (right) from January
1249 to December. Dashed-dotted horizontal line (panels b & f): hypoxia threshold (63 µM; Middelburg
1250 and Levin, 2009; Zhang et al., 2010). Vertical lines: dates of the sediment investigations. ST and
1251 NT: spring and neap tides. Color symbols: Chl *a* concentration in the first top cm of the sediment
1252 (*n = 3*).

1253

1254

37

1255 **Fig. 3** Depth profiles of the organic carbon, C_{org} (a), total nitrogen, TN (b) and C:N ratios (c) for
1256 the triplicate sediment cores at the Nord Dumet monitoring station (St. A) for the temporal study
1257 from April to September 2015. No measurements were taken on April 15th.

1258

1259

38

1260 **Fig. 4** Modeled (red curves) and measured (symbols) pore-water concentration profiles of O_2 (a),
1261 NH_4^+ (b), NO_3^- (c) and NO_2^- (d) in the temporal study from April to September 2015 conducted at
1262 the Nord Dumet monitoring station (St. A). The symbols correspond to the results from the
1263 triplicate sediment cores for the nutrients and the O_2 measurements. Dashed lines: sediment-water
1264 interface (SWI).

1265

1266

Fig. 5 Measured and simulated NH_4^+ (a), DON (b), NO_3^- (c) and NO_2^- (d) fluxes across the SWI in the Vilaine Bay during the temporal study carried out from April to September 2015 conducted at the Nord Dumet monitoring station (St. A, left) and the spatial study carried out in July 2016 (right). The error bars represent the standard error of the mean ($n = 4$). There were no model simulations for the DON fluxes.
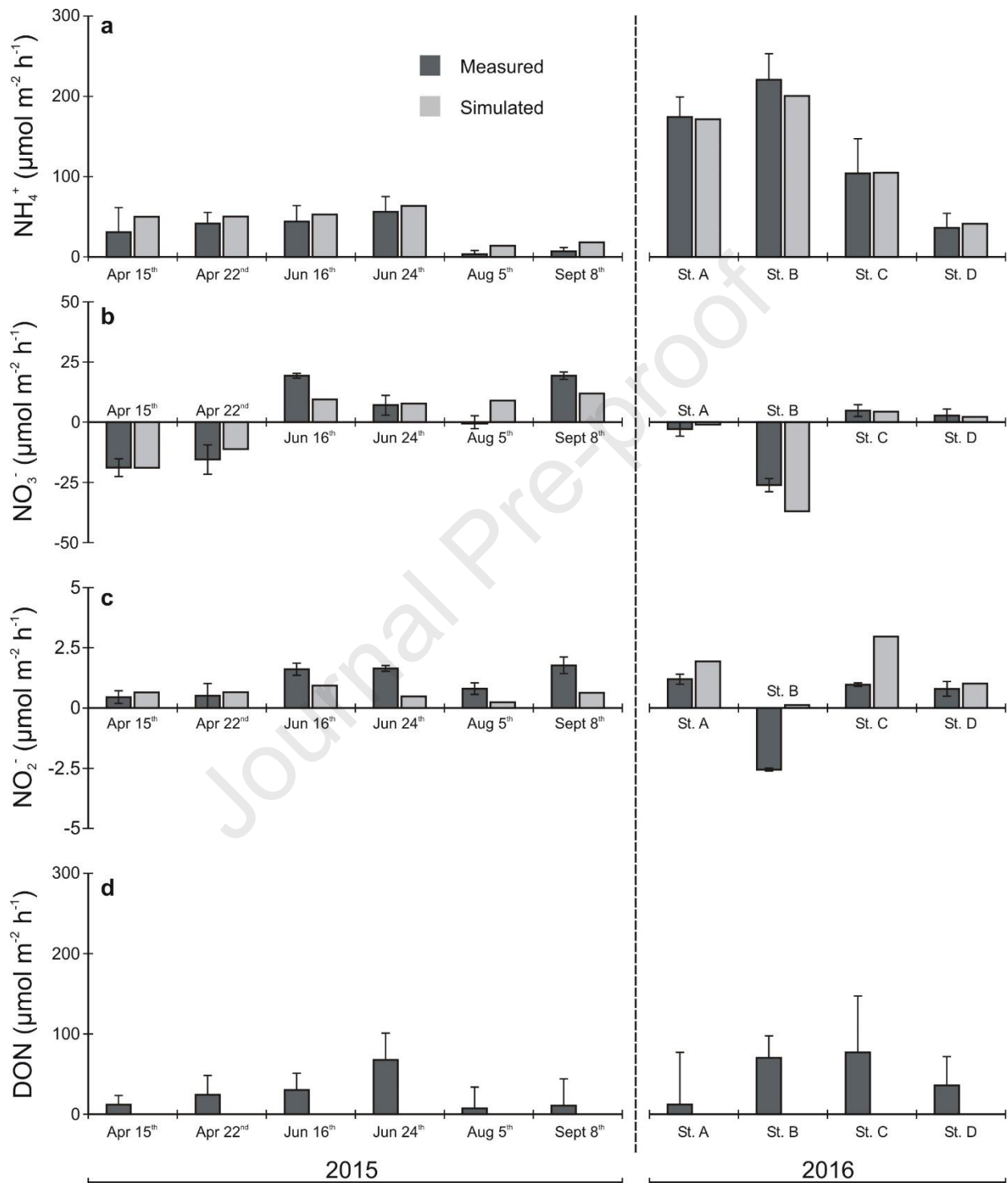
1274 **Fig. 6** Relationship between the measured NH_4^+ fluxes and Chl *a* content (a), NH_4^+ and DON
1275 fluxes (b) for the temporal study carried out in 2015. The equation and the regression line were
1276 obtained from linear regression.
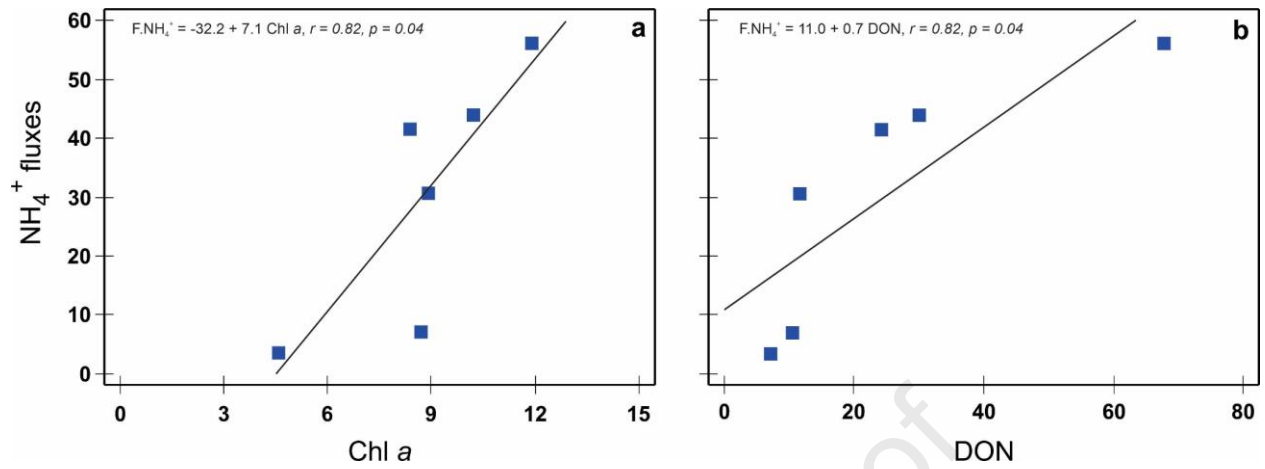
1277

1278

Fig. 7 Model sensitivity analysis showing the response of the benthic NH_4^+ fluxes during the temporal study carried out from April to September 2015 (a-f) to different scenarios of change in environmental factor-related model parameters. The response was calculated as a percentage of change in the NH_4^+ fluxes with regard to the baseline simulation (zero dashed line). The factors lying furthest from the zero dashed line are those causing the greatest change in the NH_4^+ fluxes. Anoxic: zero bottom water O_2 concentrations; BW NO_3^- = 10x [100x]: increase in the bottom water NO_3^- concentrations by 10 fold or 100 fold for August and September; OM1 2x [3x]: increase in the deposition of OM1 by 2 fold (or 3x for August); OM1 <=> OM2: inversing the proportion of OM1 and OM2; k1 OM1 = 2x: increase in the rate constant for the aerobic oxidation of OM1 by 2 fold); k1 OM1 = 1/2 x decrease in the rate constant for the aerobic oxidation of OM1 by one-half; C/N OM1 = 106/16: imposed change in the C/N ratio compared to that in living phytoplankton i.e., Redfield ratio; Db = 10x: increase in the bioturbation coefficient by 10 fold; α = 10x: increase in the bioirrigation coefficient by 10 fold.
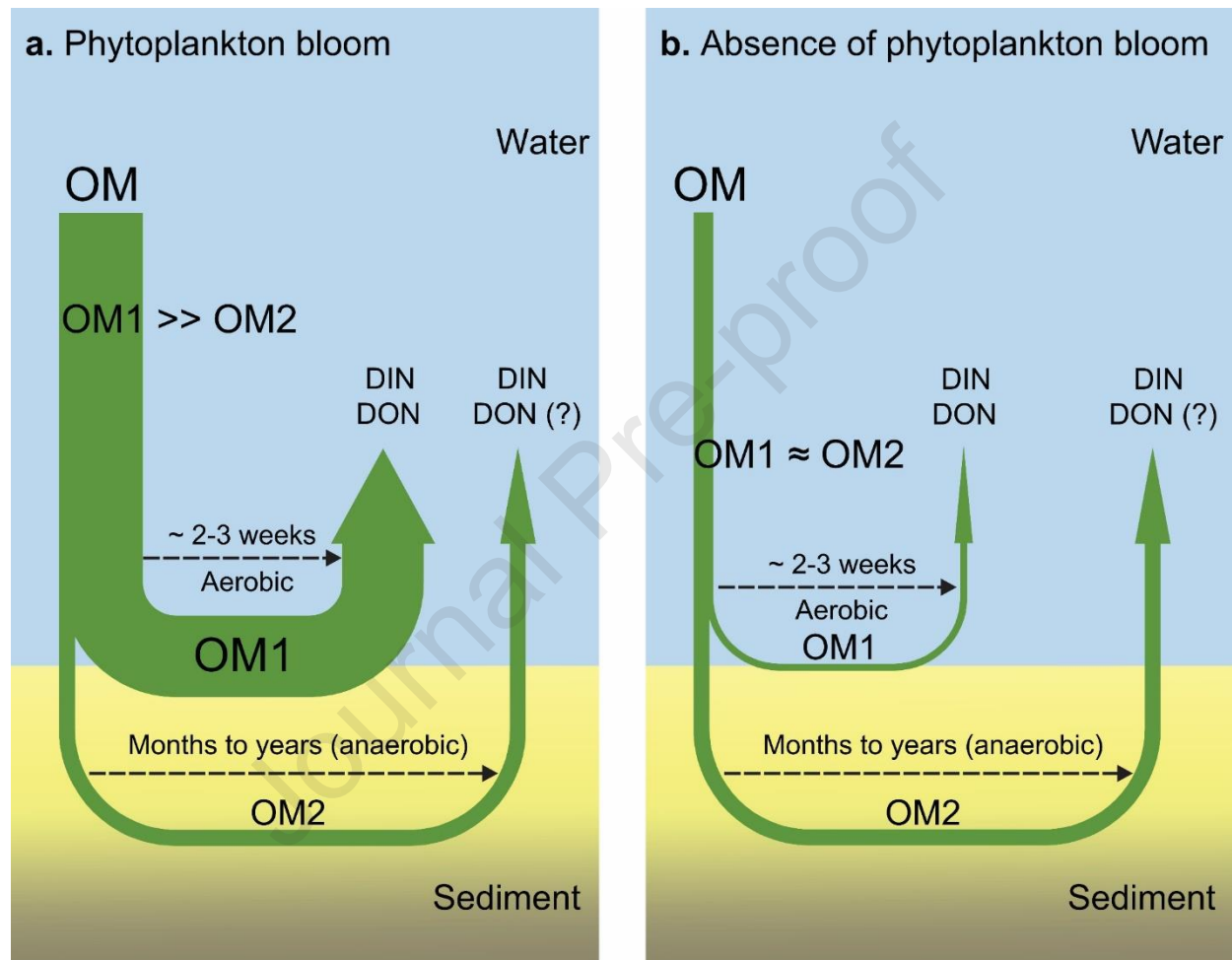
1293 **Fig. 8** Model sensitivity analysis showing the response of the benthic NO_3^- fluxes during the
1294 temporal study carried out from April to September 2015 (a-f) to different scenarios of change in
1295 environmental factor-related model parameters. The response was calculated as a percentage of
1296 change in the NO_3^- fluxes with regard to the baseline simulation (zero dashed line). The factors
1297 lying furthest from the zero dashed line are those causing the greatest change in the NO_3^- fluxes.
1298 Anoxic: zero bottom water O_2 concentrations; BW NO_3^- = 10x [100x]: increase in the bottom water
1299 NO_3^- concentrations by 10 fold or 100 fold for August and September; OM1 2x [3x]: increase in
1300 the deposition of OM1 by 2 fold (or 3x for August); OM1 <=> OM2: inversing the proportion of
1301 OM1 and OM2; k1 OM1 = 2x: increase in the rate constant for the aerobic oxidation of OM1 by
1302 2 fold); k1 OM1 = 1/2 x decrease in the rate constant for the aerobic oxidation of OM1 by one-
1303 half; C/N OM1 = 106/16: imposed change in the C/N ratio compared to that in living
1304 phytoplankton i.e., Redfield ratio; Db = 10x: increase in the bioturbation coefficient by 10 fold; α
1305 = 10x: increase in the bioirrigation coefficient by 10 fold.

1306

Fig. 9 Summary diagram of the benthic N fluxes in the Vilaine Bay for two distinct situations: (a) in the presence of a phytoplankton bloom and (b) in the absence of a phytoplankton bloom, based on field observations, laboratory measurements and a modeling study. The terms OM1 and OM2 are used to distinguish between a labile and a less labile pool of organic matter input. DIN and DON stand for dissolved inorganic and organic N, respectively. The different arrow sizes indicate the magnitude of the OM input for each pool, as well as its recycling into DIN (mostly NH_4^+) and DON. The horizontal dashed lines are meant to approximately illustrate the OM turnover time for each pathway (aerobic and anaerobic), estimated from the model rate constants of OM1 and OM2 (Table S3) and the residence time of solutes (Table S6). Where the DON diffusion from pore-water is questioned, this is indicated by a question mark.

1319   **Table 1** Model-predicted OM decomposition rates through the different pathways for OM1 and OM2 (in parentheses). All values are in μmol C m^{-2} h^{-1}

Processes	April 15th	April 22nd	June 16th	June 24th	August 5th	September 8th	St. A	St. B	St. C	St. D
O_2	475.8 (3.9)	506.4 (4.9)	605.8 (5.9)	629.7 (5.3)	261.3 (9.1)	343.3 (6.7)	1,307.9 (9.3)	1,164.4 (3.9)	862.6 (9.3)	298.9 (3.1)
NO_3^- [a]	45.5 (1.1)	36.5 (1.0)	23.1 (0.7)	19.7 (0.5)	12.9 (1.6)	17.8 (1.1)	2.6 (0.1)	49.0 (0.5)	4.6 (0.1)	4.1 (0.1)
$Fe(OH)_3$	21.3 (1.5)	21.6 (1.8)	20.9 (1.7)	20.7 (1.4)	18.1 (6.7)	19.7 (3.5)	21.1 (1.2)	20.9 (0.6)	20.7 (1.8)	23.1 (2.0)
SO_4^{2-}	111.5 (23.8)	98.7 (26.8)	133.5 (40.4)	168.5 (44.8)	19.0 (30.5)	43.0 (32.4)	354.1 (82.4)	723.1 (69.0)	238.5 (85.0)	120.0 (39.7)
Total [b]	654.1 (30.5)	663.2 (34.7)	783.3 (48.7)	838.6 (52.2)	311.3 (48.1)	423.7 (43.9)	1,685.8 (93.0)	1,957.5 (73.9)	1,126.4 (96.3)	446.2 (44.9)

1320   [a] Sum of the denitrification and DNRA rates (see section 2.4.2. and Table S1).
1321   [b] Total rates of all OM decomposition pathways.
1322

1323 **Table 2** Model-predicted depth-integrated N transformation rates derived from a model simulation. The measured potential nitrification step 1 and
1324 NO_3^- reduction rates are indicated in parentheses (mean ± SE). All values are in µmol N m^{-2} h^{-1}.

Processes	April 15th	April 22nd	June 16th	June 24th	August 5th	September 8th	St. A	St. B	St. C	St. D
Nitrification 1	18.4 (11.5 ± 0.4)	19.1 (16.7 ± 0.6)	29.2 (20.0 ± 1.6)	24.2 (28.0 ± 2.9)	20.8 (14.0 ± 2.5)	27.5 (12.0 ± 1.3)	3.1 (7.3 ± 0.7)	0.4 (0.0 ± 0.0)	7.3 (2.8 ± 0.6)	6.6 (2.2 ± 0.7)
Nitrification 2	17.7	18.3	28.2	23.7	20.5	26.8	1.1	2.0	5.4	5.5
Denitrification	35.5 (52.4 ± 6.6)	28.6 (60.7 ± 8.8)	18.1 (73.6 ± 8.2)	15.4 (119.0 ± 24.8)	11.2 (na)	14.5 (na)	2.0 (na)	37.6 (na)	3.6 (na)	3.2 (na)
DNRA	1.17	0.94	0.60	0.51	0.37	0.48	0.07	1.24	0.12	0.11
Anammox	0.08	0.10	0.06	0.06	0.08	0.07	0.04	0.06	0.03	0.05

1325

46

1326 **Supplementary materials**

1327 **Temporal and spatial variations in benthic nitrogen cycling in a temperate macro-tidal**
1328 **coastal ecosystem: observation and modeling**

1329

1330 Widya Ratmaya*[1], Anniet M. Laverman[2], Christophe Rabouille[3], Zahra Akbarzadeh[4], Françoise
1331 Andrieux-Loyer[5], Laurent Barillé[6], Anne-Laure Barillé[7], Yoann Le Merrer[1], Philippe Souchu[1]

1332

1333 [1] Ifremer – LER MPL, Rue de l'Ile d'Yeu, BP 21105, 44311 Nantes Cedex 03, France
1334 [2] Université de Rennes, CNRS, UMR 6553 ECOBIO, Campus Beaulieu, 263 avenue du Général
1335 Leclerc, Rennes F-35042, France
1336 [3] Laboratoire des Sciences du Climat et de l'Environnement, CEA-CNRS UNMR 1572, Av. de la
1337 Terrasse, 91198 Gif sur Yvette, France
1338 [4] Ecohydrology Research Group, Water Institute and Department of Earth and Environmental
1339 Sciences, University of Waterloo, 200 University Avenue West, Waterloo, Ontario, Canada
1340 [5] Ifremer – DYNECO PELAGOS, ZI Pointe du Diable, 29280 Plouzané, France
1341 [6] Université de Nantes, Mer Molécules Santé EA 2160, Faculté des Sciences et des Techniques,
1342 BP 92208, 44322 Nantes cedex 3, France
1343 [7] Bio-Littoral, Immeuble Le Nevada, 2 Rue du Château de l'Eraudière CS 80693, 44306 Nantes

1344

1345 * Email: widyaratmaya@gmail.com
1346 Laboratoire Environnement Ressource Morbihan – Pays de la Loire, Centre Ifremer de Nantes,
1347 Rue de l'Ile d'Yeu, BP 21105, 44311 Nantes Cedex 03, France.

1348   **Table S1** Reaction network and rate formulation used in the model.

Description	Reaction formulation[a]	Rate expression[b, c]
Aerobic respiration	$OM + xO_2 + (2z\text{-}y)HCO_3^- \rightarrow yNH_4^+ + zHPO_4^{2-} + (x\text{-}y+2z)CO_2 + (x\text{-}y+2z)H_2O$	$R1 = k1\,[OM] \cdot \dfrac{[O_2]}{[O_2] + kO} \cdot F_T$
Denitrification	$OM + 0.8xNO_3^- \rightarrow 0.4xN_2 + yNH_4^+ + 0.8xNO_2^- + zHPO_4^{2-} + (0.8x+y\text{-}2z)HCO_3^- + (0.2x\text{-}y+2z)CO_2 + (0.6x\text{-}y+2z)H_2O$	$R2 = k2\,[OM] \cdot \dfrac{[NO_3^-]}{[NO_3^-] + kNO} \cdot \dfrac{kinO}{[O_2] + kinO} \cdot 1 - F_{DNRA} \cdot F_T$
DNRA	$OM + 0.5xNO_3^- \rightarrow (0.5x+y)NH_4^+ + (0.5xNO_2^-) + zHPO_4^{2-} + (y\text{-}2z)HCO_3^- + (x\text{-}y+2z)CO_2 + (0.5x\text{-}y+2z)H_2O$	$R3 = k2\,[OM] \cdot \dfrac{[NO_3^-]}{[NO_3^-] + kNO} \cdot \dfrac{kinO}{[O_2] + kinO} \cdot F_{DNRA} \cdot F_T$
Nitrification step 1	$NH_4^+ + 1.5O_2 \rightarrow NO_2^- + H_2O$	$R4 = k_{nit1} \cdot \dfrac{[NH_4^+]}{[NH_4^+] + kmNH4ao} \cdot \dfrac{[O_2]}{[O_2] + kmO2ao} \cdot F_T$
Nitrification step 2	$NO_2^- + 0.5O_2 \rightarrow NO_3^-$	$R5 = k_{nit2} \cdot \dfrac{[NO_2^-]}{[NO_2^-] + khNIT} \cdot \dfrac{[O_2]}{[O_2] + khO} \cdot F_T$
Anammox	$NH_4^+ + NO_2^- \rightarrow N_2 + 2H_2O$	$R6 = k_{anx} \cdot \dfrac{[NH_4^+]}{[NH_4^+] + khNH4} \cdot \dfrac{[NO_2^-]}{[NO_2^-] + khNO} \cdot \dfrac{kinO}{[O_2] + kinO} \cdot F_T$

1349   [a] $OM = x(CH_2O)_{org} + y(NH_3)_{org} + z(H_3PO_4)_{org}$, where x, y, z represent the CNP ratios,

1350   [b] F_{DNRA} = fraction of the total nitrate reduction occurring via DNRA (5%),

1351   [c] F_T = temperature correction for the rates. $F_T = \dfrac{K_1 \cdot exp(\gamma_1 \cdot (T-T_1))}{1+K_1 \cdot exp(\gamma_1 \cdot (T-T_1))-K_1} \cdot \dfrac{K_2 \cdot exp(\gamma_2 \cdot (T_2-T))}{1+K_2 \cdot exp(\gamma_2 \cdot (T_2-T))-K_2}$, where T_1 and T_2 are the lower and upper temperature for the OM decay, respectively;

1352 K_1 and K_2 are the coefficient rates for the lower and upper temperature, respectively; γ_1 and γ_2 are the temperature rate multipliers for T_1 and T_2, respectively (see Cole and

1353   Wells, 2006 for details).

1354 **Table S2** Boundary conditions used in the model.

Parameters	Apr 15th	Apr 22nd	Jun 16th	Jun 24th	Aug 5th	Sep 8th		St. A	St. B	St. C	St. D	Unit	Sources
	2015 (Nord Dumet monitoring station/St. A)							2016					
Solutes													
O_2	142 (84%)	161 (95%)	142 (82%)	120 (75%)	118 (93%)	114 (101%)		198 (80%)	96 (37%)	170 (70%)	198 (79%)	µM	I
NO_3^-	17.7	13.1	1.60	1.30	0.07	0.04		0.37	6.82	0.20	0.47	µM	I
NO_2^-	0.27	0.26	0.12	0.17	0.03	0.03		0.04	0.73	0.00	0.06	µM	I
NH_4^+	1.90	3.30	1.03	1.23	0.21	0.09		0.80	4.40	1.80	1.61	µM	I
Fe^{2+}	0	0	0	0	0	0		0	0	0	0	µM	I
SO_4^{2-} [a]	28	28	28	28	28	28		28	28	28	28	mM	M
Solids													
OM1	600	600	700	750	275	375		1,500	1,800	1,000	400	µmol C cm^{-2} yr^{-1}	M
OM2	150	150	170	180	120	120		300	300	300	150	µmol C cm^{-2} yr^{-1}	M
$Fe(OH)_3$	75	75	75	75	75	75		75	75	75	75	µmol cm^{-2} yr^{-1}	M

1355 Solute concentrations were obtained from the measurements. Solid fluxes were constrained from the model fitting (see Methods). [a] The SO_4^{2-} concentration was constrained from
1356 the measured salinity. Sources: **M**, constrained by the model fitting; **I**, independently determined from the field data.

49

1357 **Table S3** Reaction parameter values used in the model.

Parameters	Apr 15th	Apr 22nd	Jun 16th	Jun 24th	Aug 5th	Sep 8th	St. A	St. B	St. C	St. D	Unit	Source	Ref.	Description
	2015 (Nord Dumet monitoring station/St. A)						2016							
Fixed														
C:N OM1	10	10	10	10	10	10	10	10	10	10		M		C:N ratio for OM1
C:N OM2	15	15	15	15	15	15	15	15	15	15		M		C:N ratio for OM2
k_O	5	5	5	5	5	5	5	5	5	5	μM	L	2, 4, 5	Limitation of O_2 for aerobic oxidation
k_{NO}	5	5	5	5	5	5	5	5	5	5	μM	L	2, 4, 5	Limitation of NO_3^- for denitrification
k_{mNH4ao}	5	5	5	5	5	5	5	5	5	5	μM	L	1	Limitation of NH_4^+ for nitrification step 1
k_{mO2ao}	5	5	5	5	5	5	5	5	5	5	μM	L	1	Limitation of O_2 for nitrification step 1
k_{hNIT}	1	1	1	1	1	1	1	1	1	1	μM	L	1	Limitation of NO_2^- for nitrification step 2
k_{HO}	5	5	5	5	5	5	5	5	5	5	μM	L	1	Limitation of O_2 for nitrification step 2
k_{hno}	1	1	1	1	1	1	1	1	1	1	μM	L	3	Limitation of NO_2^- for anammox
k_{hnh}	1	1	1	1	1	1	1	1	1	1	μM	L	3	Limitation of NH_4^+ for anammox
k_{inO}	6	6	6	6	6	6	6	6	6	6	μM	L	6	Inhibition of O_2 for anoxic processes
k_1 OM1	16	16	16	16	16	16	16	16	16	16	yr^{-1}	M		Rate constant for aerobic oxidation of OM1
k_1 OM2	0.1	0.1	0.1	0.1	0.1	0.1	0.1	0.1	0.1	0.1	yr^{-1}	M		Rate constant for aerobic oxidation of OM2
k_2 OM1	5	5	5	5	5	5	5	5	5	5	yr^{-1}	M		Rate constant for denitrification and DNRA of OM1
k_2 OM2	0.1	0.1	0.1	0.1	0.1	0.1	0.1	0.1	0.1	0.1	yr^{-1}	M		Rate constant for denitrification and DNRA of OM2
Adjusted														
k_{nit} 1	90	80	180	180	100	190	20	5	50	60	μmol cm^{-3} yr^{-1}	M		Maximum rate for nitrification step 1
k_{nit} 2	200	195	550	550	400	540	30	50	190	150	μmol cm^{-3} yr^{-1}	M		Maximum rate for nitrification step 2
k_{anx}	0.03	0.05	0.02	0.02	0.04	0.02	0.02	0.02	0.02	0.02	μmol cm^{-3} yr^{-1}	M		Maximum rate for anammox
Measured														
Ø	0.83	0.84	0.88	0.85	0.85	0.82	0.87	0.92	0.59	0.40	cm^3 cm^{-3}	I		Sediment porosity
ρ	2.89	2.49	3.26	2.74	3.08	3.06	2.71	4.45	2.50	1.93	g cm^{-3}	I		Sediment density
T°	11.1	11.9	14.4	14.9	17.9	17.8	16.5	13.8	17.3	15.8	°C	I		Bottom water temperature

1358 The sources of the parameter values are indicated by the following codes: **M**, constrained by the model fitting; **I**, independently determined from the field data, **L**, literature value,
1359 with references given as follows: 1. Ward (1986); 2. Wang and VanCappellen (1996); 3. Dalsgaard and Thamdrup (2002); 4. Canavan et al. (2006); 5. Dale et al. (2016); 6.
1360 Akbarzadeh et al. (2018).

1361 **Table S4** Model parameter values for the transport processes that were invariable within the season
1362 and sampling station.

Parameters	Value	Description	Unit	Sources
Db	3	Bioturbation coefficient at x < 2 cm	$cm^2\ yr^{-1}$	M
	1.5	Bioturbation coefficient at 2 cm $\leq$ x $\leq$ 4 cm	$cm^2\ yr^{-1}$	M
	0.3	Bioturbation coefficient at 4 cm $\leq$ x $\leq$ 7 cm	$cm^2\ yr^{-1}$	M
	0.1*(1 - exp(x - 20))	Bioturbation coefficient at x > 7 cm	$cm^2\ yr^{-1}$	M
α	3	Bioirrigation coefficient at x < 2 cm	yr^{-1}	M
	1.5	Bioirrigation coefficient at 2 cm $\leq$ x $\leq$ 4 cm	yr^{-1}	M
	0.3	Bioirrigation coefficient at 4 cm $\leq$ x $\leq$ 7 cm	yr^{-1}	M
	0.1*(1 - exp(x - 20))	Bioirrigation coefficient at x > 7 cm	yr^{-1}	M
ω	0.5	Burial velocity	$cm\ yr^{-1}$	M

1363 See Table S2 for the source indications
1364

51

Characteristic time-scales for the sediment processes

1. Diffusion time-scale

Diffusion time-scales calculated from the modified Einstein-Smoluchowski equation (Jørgensen and Revsbech, 1985):

$$t_{DIFF} = z^2/2D_s \qquad \text{eq. 1}$$

where t_{DIFF} is the diffusion time-scales (d), z is the characteristic length (cm), and D_s is the diffusion coefficient ($cm^2\ s^{-1}$), corrected with the bottom water temperature and sediment porosity for each measurement. The diffusion time-scale was calculated for the upper 2 cm layer, where the exchange between the sediment and overlying water occurs most actively.

Table S5 Diffusion time-scales for NH_4^+, NO_3^- and DON over the first 2 cm sediment layer.

Date	D_s NH_4^+	D_s NO_3^-	D_s DON*	t_{DIFF} NH_4^+	t_{DIFF} NO_3^-	t_{DIFF} DON
	(x 10^{-6} cm^{-2} s^{-1})			(d)		
April 15th.	1.4	1.4	0.17	1.6	1.7	13.2
April 22nd	1.4	1.4	0.18	1.6	1.6	13.2
June 16th	1.5	1.5	0.19	1.5	1.5	12.4
June 24th	1.6	1.5	0.19	1.5	1.5	12.5
August 5th	1.7	1.6	0.21	1.4	1.4	11.3
September 8th	1.7	1.6	0.21	1.4	1.4	11.1

t_{DIFF} = the diffusion time-scale; Ds = the diffusion coefficient. *The D_s of DON was estimated using the empirical relationship between the free solution diffusion coefficient (Do) and the molecular weight (MW) for the various organic compounds at 25°C in distilled water reported by Burdige et al. (1992), assuming a fixed average MW of 2500 Daltons. The obtained values were then corrected for in situ temperature using the Stoke-Einstein equation and translated to Ds after correction for sediment porosity (Boudreau, 1997).

2. Residence time of the solutes

The residence time of the solutes at steady-state can be calculated by dividing the stock of the solutes by the flux of these solutes.

$$t_{RES} = Stock/DifFlux \qquad \text{eq. 2}$$

where t_r is the residence time of the solutes (d), *Stock* is the average stock of the solutes over the first 2 cm sediment layer (μmol m^{-2}), and *DifFlux* is the diffusive fluxes of the solutes (μmol m^{-2} d^{-1}).

Table S6 Residence time of NH_4^+, NO_3^- and DON over the first 2 cm sediment layer.

Date	Stock NH_4^+	Stock NO_3^-	Stock DON	DifFlux NH_4^+	DifFlux NO_3^-	DifFlux DON	t_{RES} NH_4^+	t_{RES} NO_3^-	t_{RES} DON
	(μmol m^{-2})			(μmol m^{-2} d^{-1})			(d)		
April 15th.	3,138	376	7,473	427	-247	148	7.4	1.5	50
April 22nd	3,699	294	8,156	541	-99	157	6.8	3.0	52
June 16th	3,487	130	6,471	518	17	175	6.7	7.5	37
June 24th	2,858	198	9,469	439	44	225	6.5	4.5	42
August 5th	3,384	84	6,322	589	21	193	5.7	4.1	33
September 8th	3,795	113	6,916	567	22	212	6.7	5.2	33

* Diffusive fluxes calculated from the concentration gradient at the SWI using Fick's first law of diffusion (Boudreau, 1997; Schulz, 2006)

1390 **Sensitivity analysis**

1391   The sensitivity analysis was carried out by imposing changes in the model boundary
1392 condition (Table S3) and parameter values (Table S2 & S4) for each sampling date. The
1393 contribution of NO_2^- to the DIN fluxes was considered negligible (< 5% of the NH_4^+ and NO_3^-
1394 fluxes) and therefore it not included in the sensitivity analysis. A stepwise approach was applied
1395 by manually changing the parameter values individually (Table S7) and observing the model
1396 response on the NH_4^+ and NO_3^- fluxes. The model was run by imposing each change in these
1397 values one by one for each sampling date. A combination effect between the parameters was not
1398 tested in the sensitivity analysis in the present study. The response was calculated as a percentage
1399 of change in the NH_4^+ and NO_3^- fluxes with regard to best fits (baseline model).

1400 **Table S7** List of tested parameters for the sensitivity analysis.

Parameters	Description
Anoxic	Bottom water O_2 concentrations are equal to zero
BW NO_3^- = 10x (100x)	Increase in the bottom water NO_3^- concentrations by 10 fold (or 100 fold for August and September)
OM1 2x (3x)	Increase in the deposition of OM1 by 2 fold (or 3x for August)
OM1 <=> OM2	Inversing the proportion of OM1 and OM2
k_1 OM1 = 2x	Increase in the rate constant for the aerobic oxidation of OM1 by 2 fold
k_1 OM1 = 1/2 x	Decrease in the rate constant for the aerobic oxidation of OM1 by one-half
C/N OM1 = 106/16	Imposed change in the C/N ratio compared to that in living phytoplankton (i.e., Redfield ratio)
Db = 10x	Increase in the bioturbation coefficient by 10 fold
α = 10x	Increase in the bioirrigation coefficient by 10 fold

1401

1402 **Table S8** Density of macrofauna in the incubated sediment cores ($n = 6$) of the temporal study
1403 carried out at the ND monitoring station in 2015.

Taxa / Species names	Apr 15th	Apr 22nd	Jun 16th	Jun 24th	Aug 5th	Sep 8th
Crustacea						
Asthenognathus atlanticus	1	2				
Philocheras bispinosus bispinosus			1			
Echinoderms						
Acrocnida brachiata	1				1	
Amphiura filiformis	6	6	4	22		6
Labidoplax digitata					2	
Leptopentacta elongata			1	2	2	
Synaptidae						
Molluscs						
Abra nitida			1		2	1
Corbula gibba		1				
Kurtiella bidentata	5		1	3		4
Nassarius pygmaeus					1	1
Nucula nitidosa	27	27	15	24	3	5
Philine aperta				1	2	
Spisula solida	1					
Turritella communis				1	1	
Annelids						
Aphelochaeta						1
Chaetozone						1
Glycera unicornis	1					1
Heteromastus filiformis		2				6
Labioleanira yhleni	1	4	2	2	1	
Magelona			1		4	
Maldanidae		1	1	4	1	
Malmgrenia lilianae	3	1		3		
Nephtys	1	1				
Pholoe baltica			1	1		
Sternaspis scutata	5	3	5	1	8	
Cnidaria						
Edwardsidae					1	
Halcampa						
Virgularia					1	4
Others						
Nemertea		2	1			1
Phoronidien		1				1
[a] Average value (Ind. m^{-2})	1354	1328	886	1667	781	833

1404 * Sediment core surface area = 64 cm^2; [a] Average value for 6 sediment cores

54

1405 Table S9. Spearman's rank correlations between benthic macrofauna density, N transformation
1406 rates, benthic N fluxes bottom water turbidity and O_2 concentration for the temporal study in 2015
1407 ($n = 6$). Asterisks designate significant correlations ($***$ p <0.001, $**$ p <0.01, $*$ p <0.05).

	NTF1	NTF2	DNF	DNRA	ANX	AMF	F.NO$_3^-$	F.NH$_4^+$	Fauna	Turb	Oxy
NTF1	1.00										
NTF2	1.00***	1.00									
DNF	-0.49	-0.49	1.00								
DNRA	-0.49	-0.49	1.00***	1.00							
ANX	-0.79	-0.79	0.26	0.26	1.00						
AMF	0.26	0.26	0.43	0.43	-0.53	1.00					
F.NO$_3^-$	0.89*	0.89*	-0.71	-0.71	-0.53	-0.20	1.00				
F.NH$_4^+$	0.23	0.23	0.46	0.46	-0.58	0.99*	-0.23	1.00			
Fauna	-0.31	-0.31	0.66	0.66	-0.18	0.77	-0.66	0.81	1.00		
Turb	-0.90*	-0.90*	0.64	0.64	0.72	-0.12	-0.90*	-0.09	0.29	1.00	
Oxy	-0.03	-0.03	-0.41	-0.41	0.31	-0.93*	0.41	-0.90*	-0.75	-0.13	1.00

1408 NTF1: Nitrification step 1; NTF2: Nitrification step 2; DNF: Denitrification; ANX: Anammox; AMF:
1409 Ammonification; F.NO$_3^-$: NO$_3^-$ fluxes; F.NH$_4^+$: NH$_4^+$ fluxes; Fauna: Macrofauna density: Turb & Oxy: bottom water
1410 turbidity (NTU) and oxygen concentration (µM) respectively.
1411

55

References

Akbarzadeh, Z., Laverman, A.M., Rezanezhad, F., Raimonet, M., Viollier, E., Shafei, B., Van Cappellen, P., 2018. Benthic nitrite exchanges in the Seine River (France): An early diagenetic modeling analysis. Sci. Total Environ. 628-629, 580-593. https://dx.doi.org/10.1016/j.scitotenv.2018.01.319.

Boudreau, B.P., 1997. Diagenetic Models and Their Implementation : Modelling Transport and Reactions in Aquatic Sediments. Springer-Verlag, Berlin.

Burdige, D.J., Alperin, M.J., Homstead, J., Martens, C.S., 1992. The role of benthic fluxes of dissolved organic carbon in oceanic and sedimentary carbon cycling. Geophys. Res. Lett. 19, 1851-1854. https://dx.doi.org/10.1029/92gl02159.

Canavan, R.W., Slomp, C.P., Jourabchi, P., Van Cappellen, P., Laverman, A.M., van den Berg, G.A., 2006. Organic matter mineralization in sediment of a coastal freshwater lake and response to salinization. Geochim. Cosmochim. Ac. 70, 2836-2855. https://dx.doi.org/10.1016/j.gca.2006.03.012.

Cole, T.M., Wells, S.A., 2006. CE-QUAL-W2: A Two-Dimensional, Laterally Averaged, Hydrodynamic and Water Quality Model, Version 3.5. User Manual. p. 680.

Dale, A.W., Sommer, S., Lomnitz, U., Bourbonnais, A., Wallmann, K., 2016. Biological nitrate transport in sediments on the Peruvian margin mitigates benthic sulfide emissions and drives pelagic N loss during stagnation events. Deep Sea Research Part I: Oceanographic Research Papers 112, 123-136. 10.1016/j.dsr.2016.02.013.

Dalsgaard, T., Thamdrup, B., 2002. Factors controlling anaerobic ammonium oxidation with nitrite in marine sediments. Appl Environ Microbiol 68, 3802-3808. https://dx.doi.org/10.1128/aem.68.8.3802-3808.2002.

Jørgensen, B.B., Revsbech, N.P., 1985. Diffusive boundary layers and the oxygen uptake of sediments and detritus1. Limnol. Oceanogr. 30, 111-122. https://dx.doi.org/10.4319/lo.1985.30.1.0111.

Schulz, H.D., 2006. Quantification of Early Diagenesis: Dissolved Constituents in Pore Water and Signals in the Solid Phase. In: Schulz, H.D., Zabel, M. (Eds.), Marine Geochemistry. Springer Berlin Heidelberg, Berlin, Heidelberg, pp. 73-124. https://dx.doi.org/10.1007/3-540-32144-6_3.

Wang, Y.F., VanCappellen, P., 1996. A multicomponent reactive transport model of early diagenesis: Application to redox cycling in coastal marine sediments. Geochim. Cosmochim. Ac. 60, 2993-3014. https://dx.doi.org/10.1016/0016-7037(96)00140-8.

Ward, B.B., 1986. Nitrification in Marine Environments. In: Prosser, J.I. (Ed.), Nitrification. IRL Press, Oxford, pp. 157-184.

1448 **Fig. S1** Sediment core incubations for measuring benthic DIN and DON fluxes in the laboratory.
1449 Two triplicates were incubated in dark and the light conditions, respectively; a control core without
1450 sediment was used to monitor the evolution of the overlying water itself.

1451

1452

1453 **Fig. S2** Variations in the salinity and river discharge (Loire and Vilaine) (a, e), temperature and
1454 dissolved O$_2$ (b, f), NO$_3^-$ + NO$_2^-$ and NH$_4^+$ (c, g), Chl *a* in the water column and sediment surface
1455 (d, h), at the Ouest Loscolo monitoring station in 2015 (left) and 2016 (right) from January to
1456 December. Dashed-dotted horizontal line (panels a & e): hypoxia threshold (63 µM; Middelburg
1457 and Levin, 2009; Zhang et al., 2010). Vertical lines: dates of the sediment investigations.

1458
1459

58
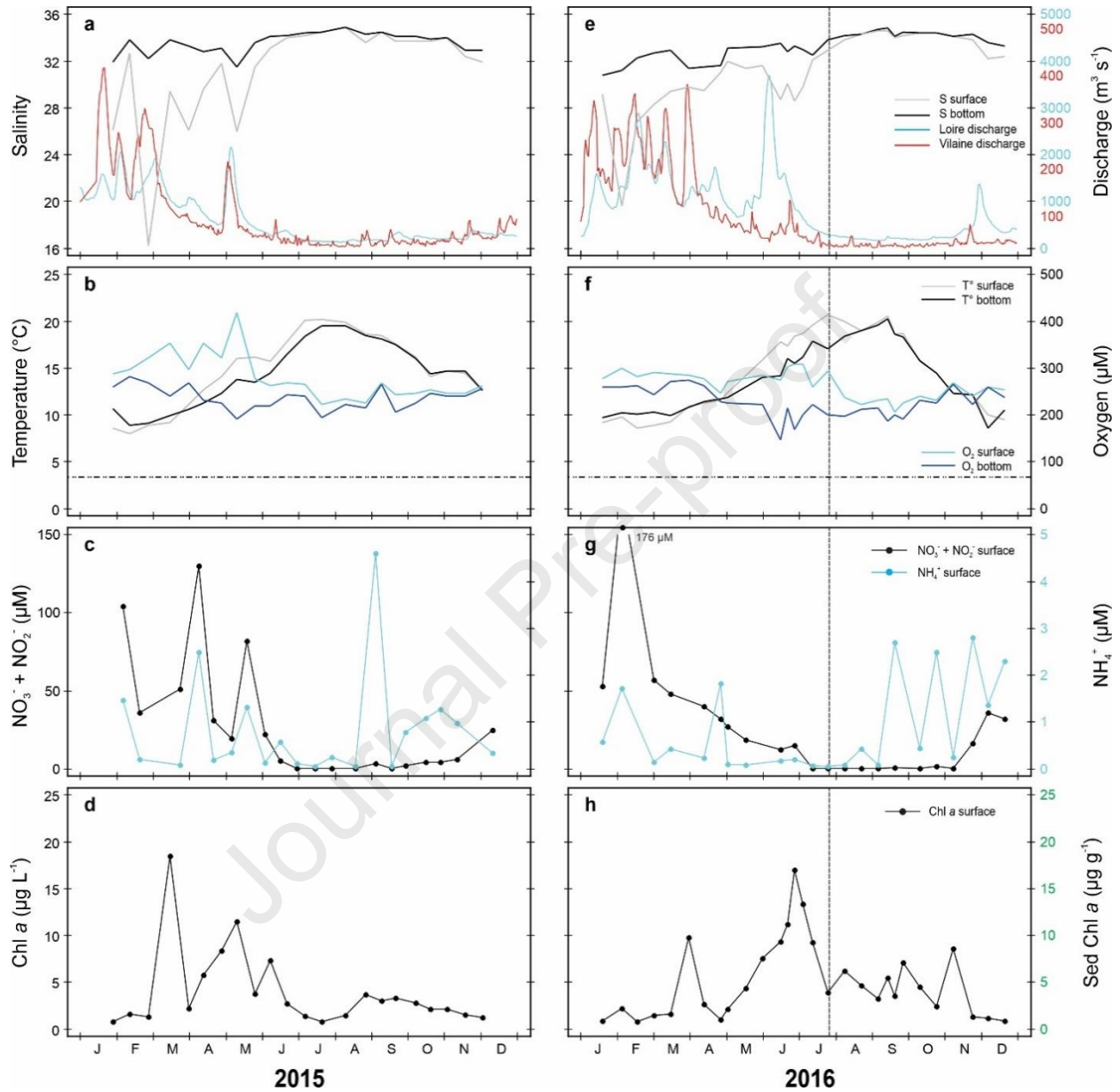
Fig. S3 Depth profile of the grain size distribution at the Nord Dumet monitoring station (St. A) in triplicate sediment cores for the temporal study from April to September 2015. The y-axis represents each section of the sediment layers in the triplicate cores.

59
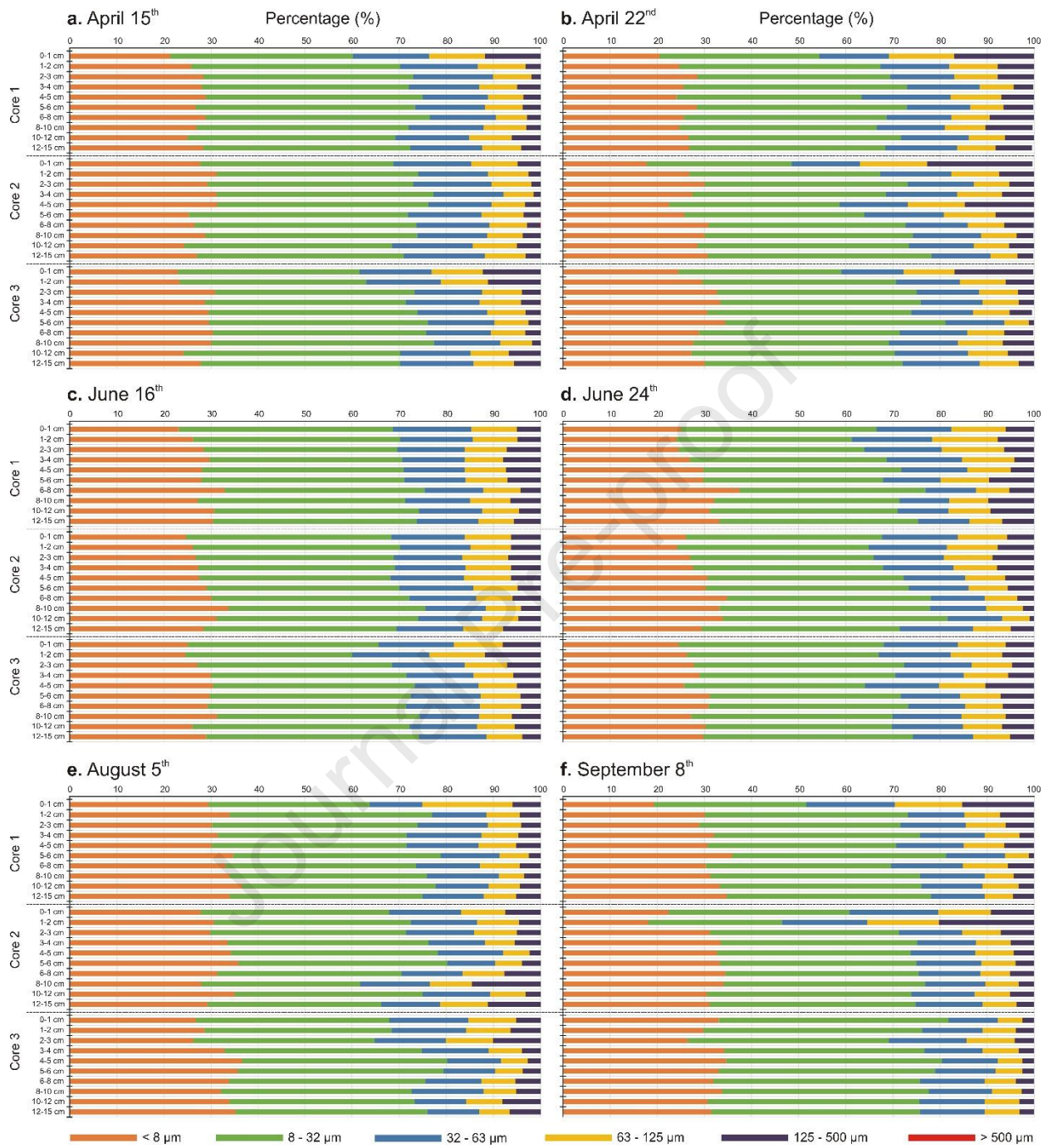
Fig. S4 Depth profile of the grain size distribution in the triplicate sediment cores at Station A, B & C for the spatial study carried out in July 2016. The y-axis represents each section of the sediment layers in the triplicate cores. Right panel: image of a sediment core sampled at Station D. There was no analysis of the grain size distribution for Station D.
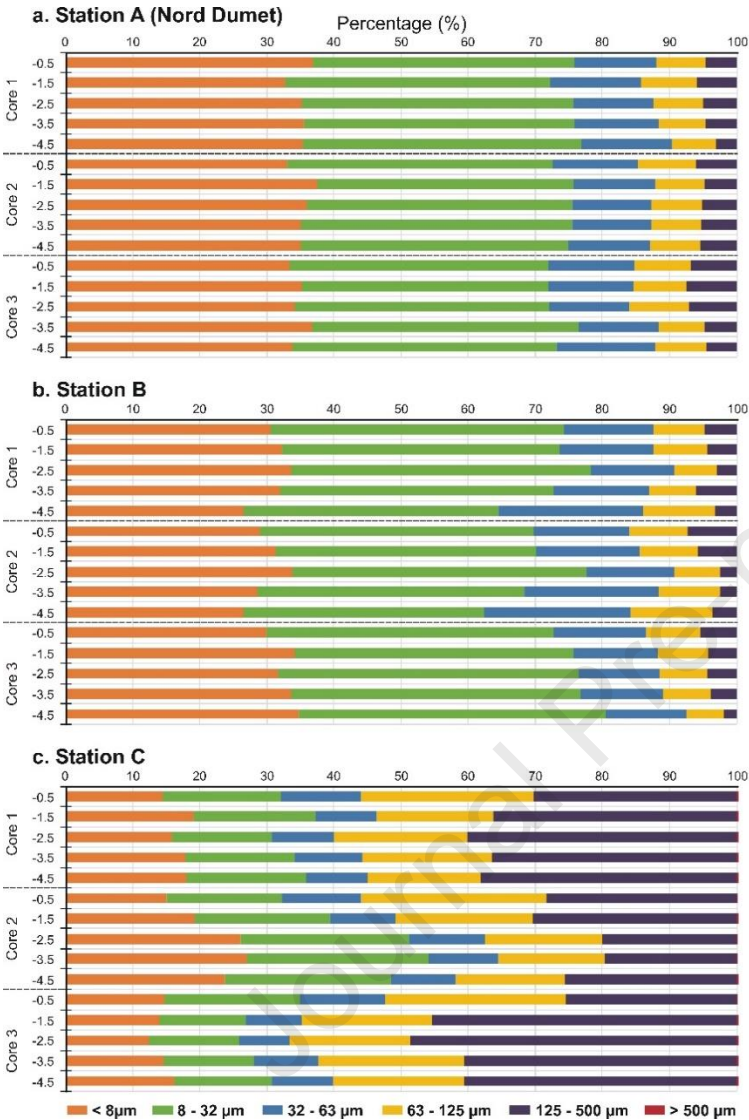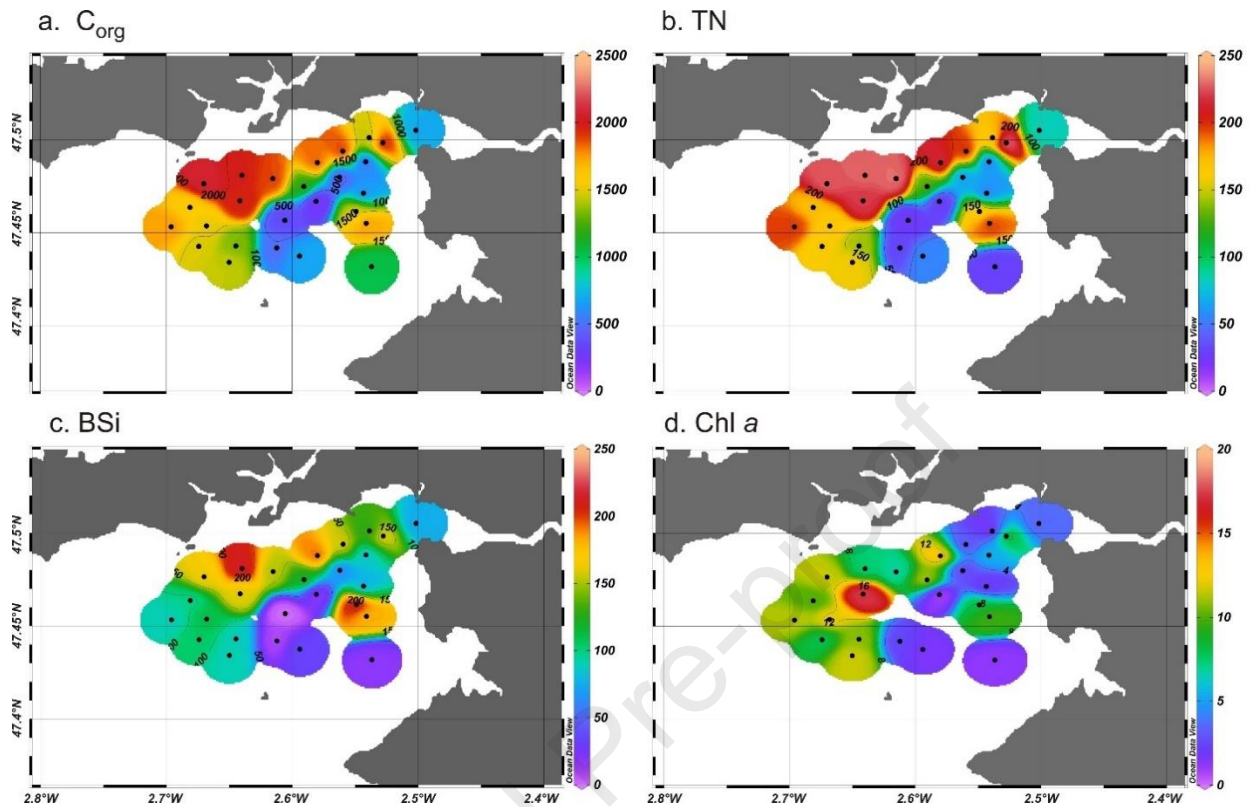
1471 **Fig. S5** Depth profiles of the sediment porosity (a) and density (b) at the Nord Dumet monitoring
1472 station (St. A) for the temporal study carried out from April to September 2015. The solid
1473 horizontal lines are the standard error of the triplicate sediment cores. The red curves are the
1474 average of all values with the standard error ($n = 60$).

1475
1476

61
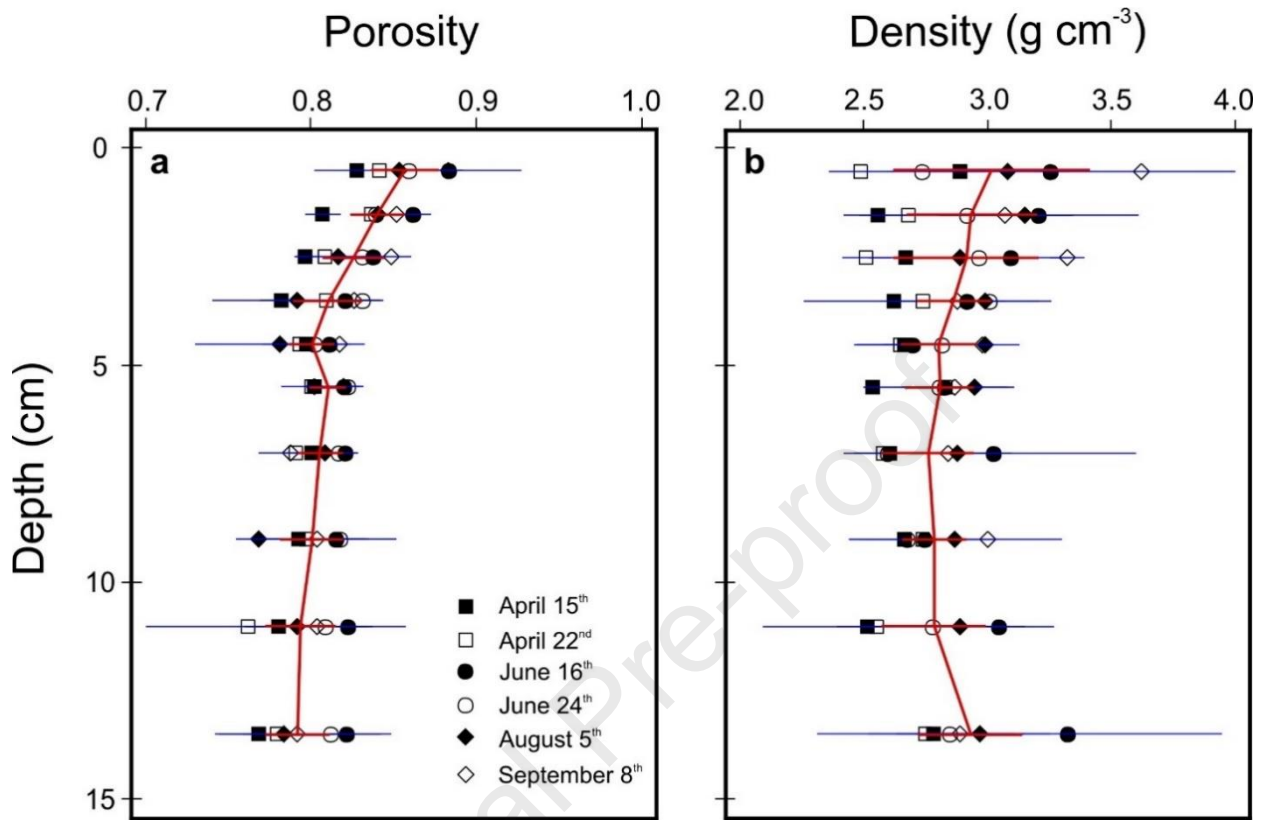
1477 **Fig. S6** Depth profiles of the sediment porosity (a) and density (b) at Station A, B & C for the
1478 spatial study carried out in July 2016. The solid horizontal lines are the standard error of the
1479 triplicate sediment cores. Note: there was no measurement for Station D (gravel).

1480

1481
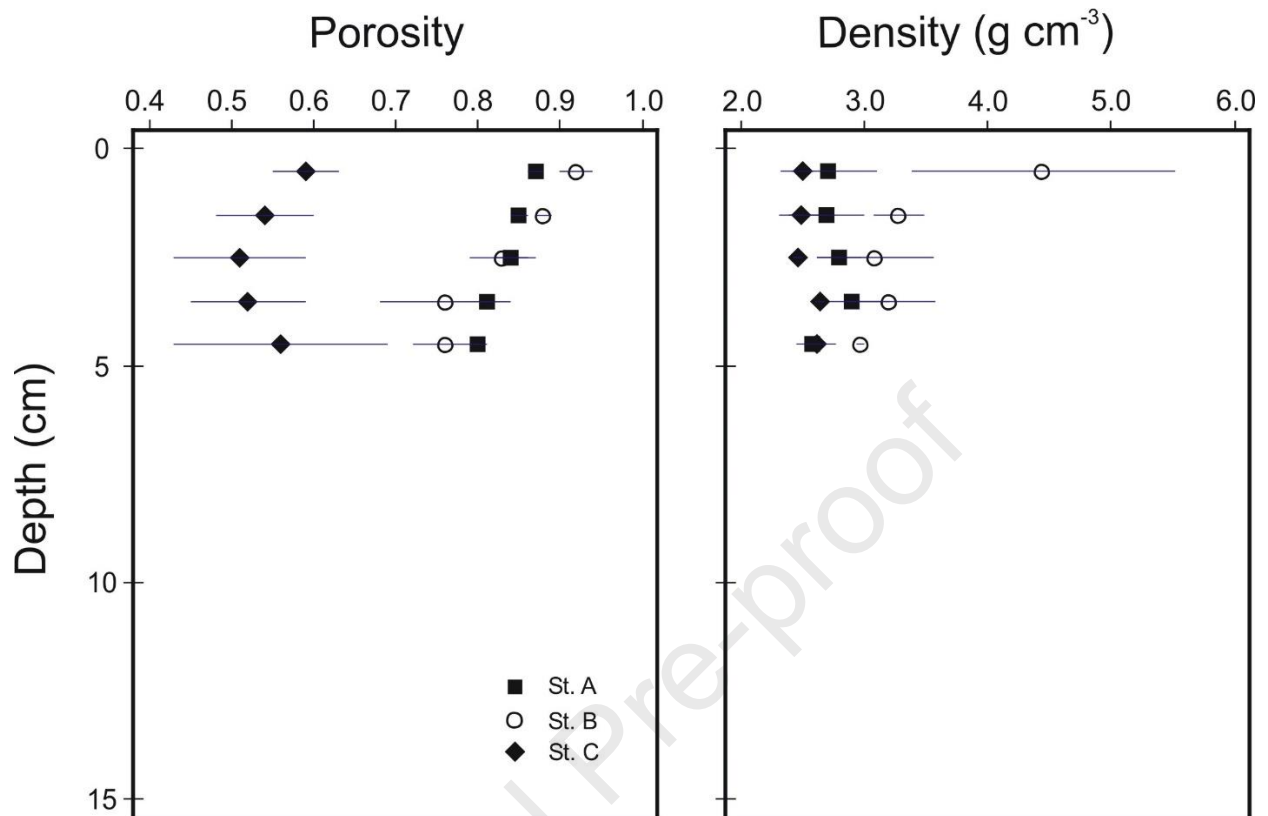
1482 **Fig. S7** C_{org}, total N, BSi (in µmol g^{-1}) and Chl *a* (in µg g^{-1}) concentrations at the sediment surface
1483 (5 cm and 1 cm for Chl *a*) in April 2016. The data were interpolated using an automatic weighted-
1484 average gridding with the Ocean Data View software.

1485

1486

1487 **Fig. S8** DON depth profiles at the Nord Dumet monitoring station (St. A) for the temporal study
1488 carried out from April to September 2015 (a) and global average of the measured DON and NH_4^+
1489 values (b). The solid horizontal lines are the standard error of the triplicate sediment cores.


1490

1491
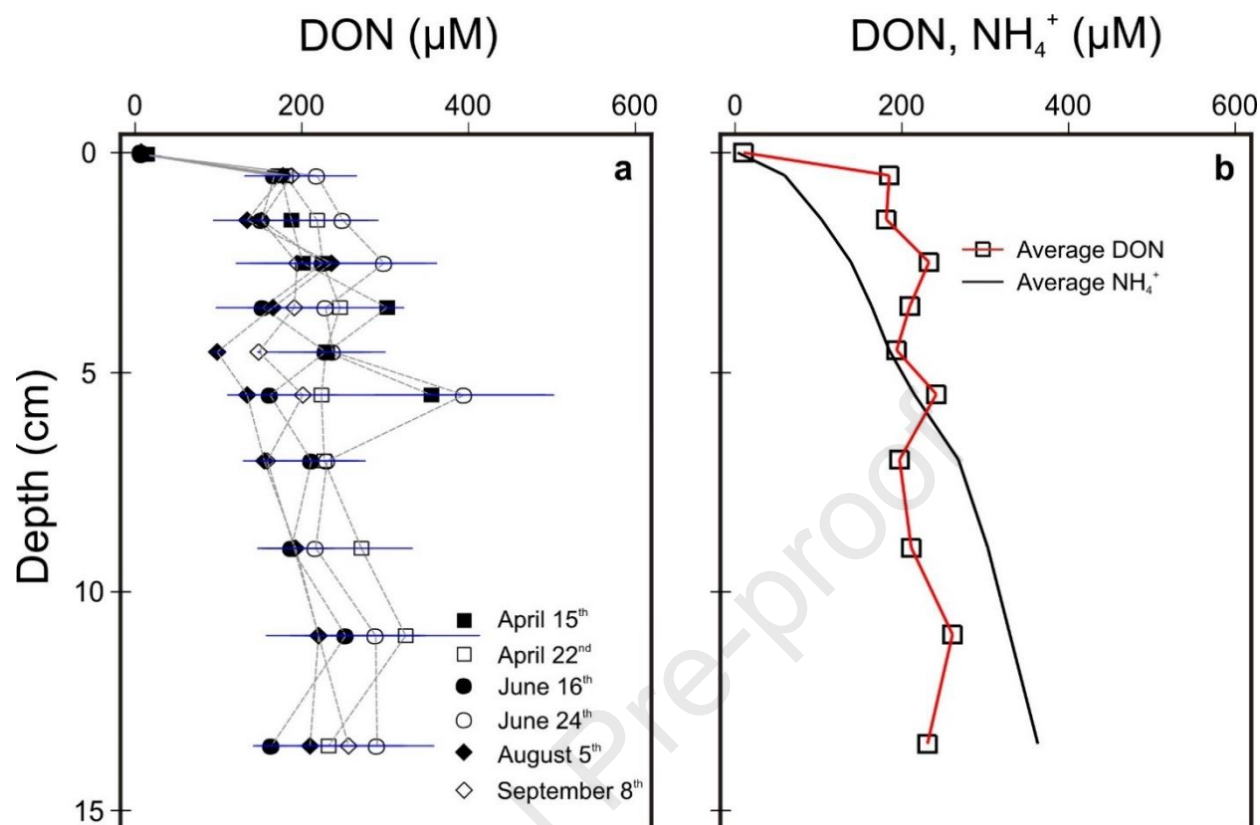
1492 **Fig. S9** Microscopic observation of microalgae cells on the surface sediment at the Nord Dumet
1493 monitoring station (St. A) during the period of study from April to June (a) and from August to
1494 September (b) 2015.

1495

1496

1497
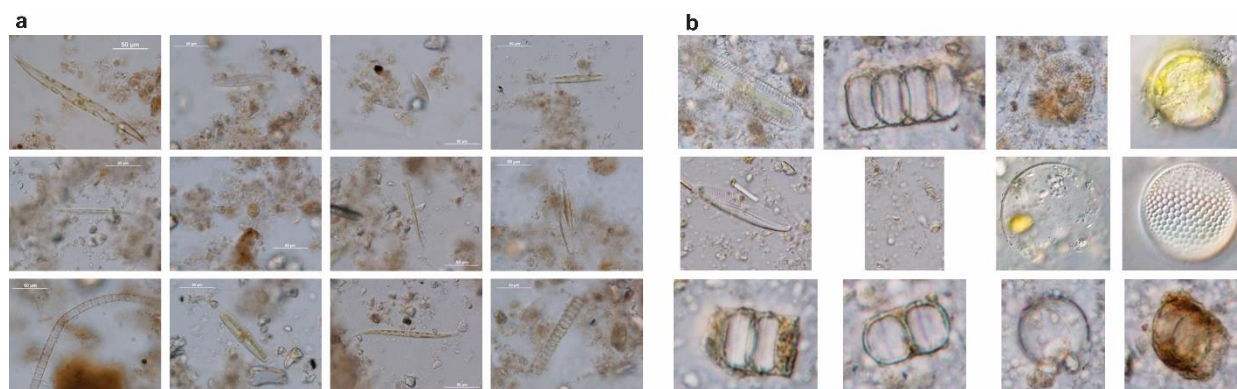
1498   **Fig. S10** Modeled NH_4^+ fluxes in 2015 across the SWI as a function of the various fDNRA values.
1499   Sampling dates are represented by the various colored lines with color symbols. Solid symbols
1500   represent the NH_4^+ fluxes measured at the Nord Dumet station.
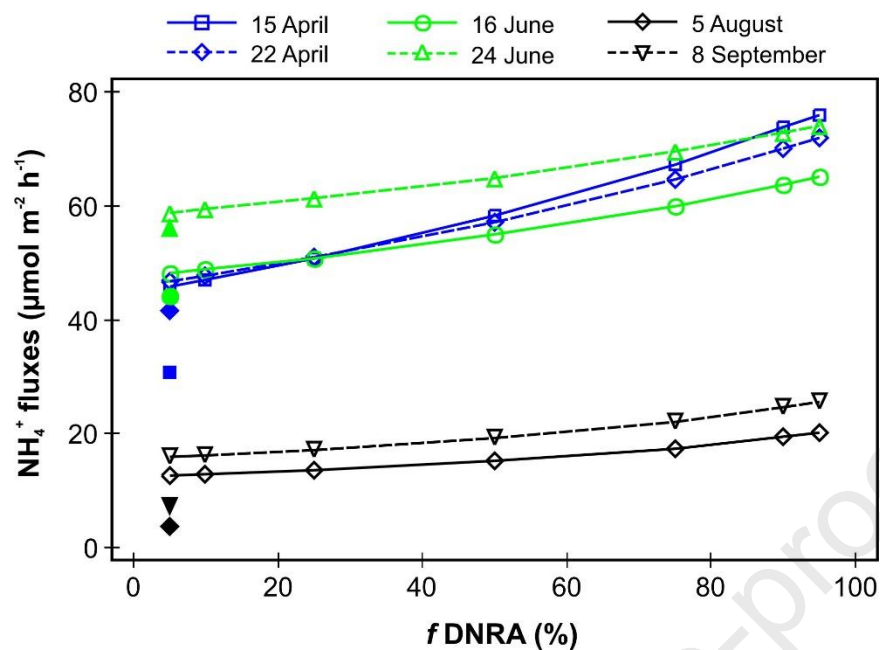
1501

1502

- The temporal and spatial variations of benthic N cycling in a eutrophic macro-tidal bay are studied using field measurements and the reactive transport model

- Benthic N flux variations depend on the phytoplankton-derived organic matter input

- Rapid mineralization of organic matter at the sediment-water interface controls benthic N cycling dynamics and sediment oxygen consumption

- Organic matter decomposition can be followed by bottom water hypoxia when blooms occur in the summer

Declaration of interests

☒ The authors declare that they have no known competing financial interests or personal relationships that could have appeared to influence the work reported in this paper.

☐The authors declare the following financial interests/personal relationships which may be considered as potential competing interests: